



A clockwise P-T-t-D path of the northern Patagonia basement: implications for the Permian evolution of the Panthalassan margin of Gondwana

Pablo D. González, Sebastián Oriolo, Bernhard Schulz, Maximiliano Naipauer, Paulo Marcos, Emiliano Renda, María Cecilia Cávana & Joachim Krause

To cite this article: Pablo D. González, Sebastián Oriolo, Bernhard Schulz, Maximiliano Naipauer, Paulo Marcos, Emiliano Renda, María Cecilia Cávana & Joachim Krause (05 Jul 2024): A clockwise P-T-t-D path of the northern Patagonia basement: implications for the Permian evolution of the Panthalassan margin of Gondwana, International Geology Review, DOI: [10.1080/00206814.2024.2375727](https://doi.org/10.1080/00206814.2024.2375727)

To link to this article: <https://doi.org/10.1080/00206814.2024.2375727>



View supplementary material [↗](#)



Published online: 05 Jul 2024.



Submit your article to this journal [↗](#)



View related articles [↗](#)



View Crossmark data [↗](#)



A clockwise P-T-t-D path of the northern Patagonia basement: implications for the Permian evolution of the Panthalassan margin of Gondwana

Pablo D. González^a, Sebastián Oriolo^b, Bernhard Schulz^c, Maximiliano Naipauer^d, Paulo Marcos^e, Emiliano Renda^e, María Cecilia Cábana^e and Joachim Krause^f

^aCONICET-SEGEMAR-UNRN, Centro SEGEMAR General Roca, General Roca, Argentina; ^bDepartment of Geological Sciences, Instituto de Geociencias Básicas, Aplicadas y Ambientales de Buenos Aires (UBA-CONICET), Buenos Aires, Argentina; ^cInstitute of Mineralogy, Division of Economic Geology and Petrology, TU Bergakademie Freiberg, Freiberg, Germany; ^dInstituto de Geocronología y Geología Isotópica, Departamento de Ciencias Geológicas, FCEN, Universidad de Buenos Aires-CONICET, Buenos Aires, Argentina; ^eUNRN, Sede Alto Valle-Valle Medio. Instituto de Investigación en Paleobiología y Geología (UNRN-CONICET), General Roca, Argentina; ^fHelmholtz-Zentrum Dresden-Rossendorf, Helmholtz Institut Freiberg für Ressourcentechnologie, Freiberg, Germany

ABSTRACT

The geologic evolution of the Gondwanide orogen recorded during the late Palaeozoic along the Panthalassan border of Gondwana is related to an active continental margin, though it is still debatable whether it was built by collision or accretion. To disentangle its orogenic processes and provide constraints on the orogen type, we characterize the physicochemical conditions of metamorphism and associated deformation of the Mina Gonzalito Metamorphic Complex from northern Patagonia (41°28'30" S-65°40'30" W). New field mapping and comprehensive petrochronologic analysis constrain the evolution of a thick-skinned fold and thrust belt in a retroarc setting, which is spatially and temporally related to the geometry and kinematics of the right-lateral reverse El Jagüelito ductile shear zone. Metamorphic evolution resulted in a clockwise P-T-t-D path reflecting three stages of continuously changing P-T conditions under high-pressure (8.0–9.9 kbar) amphibolite facies (540–680°C) during a single-phase progressive ductile deformation event. Monazite ages ranging from 303 ± 5 to 252 ± 6 Ma account for the single-phase regional tectono-metamorphic event spanning ~ 50 My. Our results, integrated with regional data, led to interpreting the late Palaeozoic Gondwanide orogen developed along the Panthalassan margin of Gondwana as accretionary in advancing-mode.

ARTICLE HISTORY

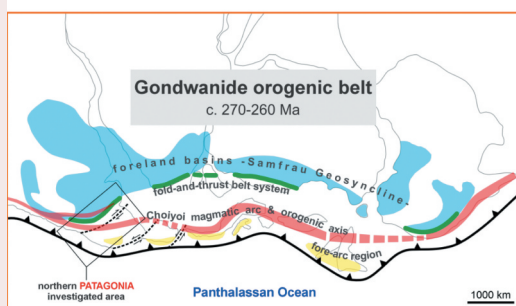
Received 21 April 2024
Accepted 29 June 2024

KEYWORDS

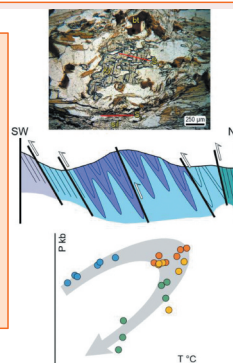
Geothermobarometry;
petrochronology; monazite;
late Palaeozoic

A clockwise P-T-t-D path of the northern Patagonia basement: Implications for the Permian evolution of the Panthalassan margin of Gondwana

single-phase progressive deformation & high-P amphibolite facies metamorphism




Field mapping
Petrography
EPMA U-Th-Pb
monazite dating
Thermobarometry



advancing-mode accretionary Gondwanide orogen along the continental margin

González, P.D., Oriolo, S., Schulz, B., Naipauer, M., Marcos, P., Renda, E., Cábana, M.C., Krause, J., 2024, *International Geology Review*

CONTACT Pablo D. González  pdgonzalez@unrn.edu.ar; pablo.diego.gonzalez@gmail.com  CONICET-SEGEMAR-UNRN, Centro SEGEMAR General Roca, Independencia 1487, Parque Industrial 1, General Roca CP 8332, Argentina

 Supplemental data for this article can be accessed online at <https://doi.org/10.1080/00206814.2024.2375727>.

© 2024 National Scientific and Technical Research Council of Argentina

Introduction

The pre-Carboniferous crystalline basement of central-northern Patagonia involved in the late Palaeozoic Gondwanide orogen follows NW-SE trending belt between 39°S–72°W and 44°S–68°W, along the Panthalassan (SW Palaeo-Pacific) margin of Gondwana (Figure 1(a,b)). This basement comprises low- to high-grade metamorphic rocks with polyphase deformation and subduction-related granitoid plutons. U-Pb zircon, geochemical, and isotopic data led to magmatism distribution episodically within Devonian, Carboniferous, and Permian (Varela et al. 2005, 2014; Pankhurst et al. 2006, 2014; Hervé et al. 2018; Gregori et al. 2021; Rapela et al. 2024). The tectono-metamorphic processes are regional, alternating with lulls of magmatic activity (Renda et al. 2021; Falco et al. 2022; Marcos et al. 2023; Oriolo et al. 2023). Either a terrane collision or accretion linked to transpression related to advancing-retreating subduction built the Gondwanide orogen (see below geotectonic models).

Despite its importance for assessing the nature of the Gondwanide orogen in Patagonia, robust constraints on physical conditions and the timing of tectono-metamorphic events are scarce. Since the interpretation of geochronological data is not straightforward, independent lines of evidence are required to evaluate radiometric data regarding geologically meaningful ages, particularly for complexly deformed metamorphic rocks. Field geologic and structural data combined with microstructural information are also crucial, providing unique constraints for reconstructing regional tectono-metamorphic processes (Bosse and Villa 2019; Oriolo et al. 2022). Monazite petrochronology is vital to determining the age of orogenic processes, as well as its chemical and isotopic composition help disentangle complex zonation patterns and the presence of different populations arising from various igneous and metamorphic events (Engi 2017; Schulz 2021).

The focus of this contribution is to characterize the metamorphic conditions and associated deformational structures of the Gondwanide crystalline basement from northern Patagonia (41°28'30" S–65°40'30" W, Figure 1(b)). New structural, microstructural, petrologic, and electron probe microanalysis Th-U-Pb monazite data from schists constrain its P-T-t-D path. Based on these results, we present a revised scheme for the regional evolution of the Gondwanide orogen in South America, providing insights into the coupled evolution of the late Palaeozoic rocks. We also review and evaluate the implications of the possible geotectonic scenarios of this orogen along the Panthalassan Gondwana margin, especially concerning crustal thickening resulting from either a terrane collision or subduction-related accretionary processes.

Geologic setting

The Gondwanide orogen is a late Palaeozoic–Early Triassic Andean-type continental mountain chain developed along the Panthalassan Gondwana margin from South America to Eastern Australia, encompassing South Africa, Malvinas Islands, Ellsworth-Whitmore Mountains, Antarctic Peninsula, Transantarctic Mountains, and Zealandia (e.g. López-Gamundí and Rossello 1998; Trouw and de Wit 1999). The orogenic belt would have been contiguous and collinear before the dispersal of Gondwana into continental fragments since the Late Triassic–Early Jurassic. It integrated the final stages of the Terra Australis orogen, which was part of the more extended (~18000 km long) and protracted (Neoproterozoic–Permian) active continental margin known along the western Gondwana border (Cawood 2005). The supercontinent interior recorded orogenic activity related to basin formation, tectono-metamorphic processes, and magmatism development up to ~1300 km inboard of the inferred continental margin located southward (Figure 1(a), Trouw and de Wit 1999).

The orogen involved the late Palaeozoic sediments of the foreland 'Samfrau Geosyncline' basin (Du Toit 1927). The 'Gondwanide Foldings' (Du Toit 1937) describe the Gondwanide deformation of the Samfrau Geosyncline consisting of asymmetric folding, thrusting, and cleavage formation along and across the orogen. This continental-scale Gondwanide fold-thrust belt system includes segments preserved in the Sierra de la Ventana in South America, the Cape Belt of South Africa, Malvinas Islands, Ellsworth-Whitmore and Pensacola Mountains of West Antarctica, and New England in Australia, among others (e.g. López-Gamundí and Rossello 1998; Trouw and de Wit 1999).

The extensive intermediate to acid Choiyoi Magmatic Province accompanies the fold-thrust belt system to the west along the continental margin, representing the Gondwanide arc magmatism (Figure 1(a); Kay et al. 1989; Sato et al. 2015). The Choiyoi volcanism is generally regarded as the source for the widespread ash fall deposits interlayered in sedimentary sequences of the coeval retroarc, foreland, and intracontinental basins (Samfrau Geosyncline), such as the adjacent Sauce Grande, Paraná and, Karroo basins, among others (Rocha-Campos et al. 2011; Sato et al. 2015).

The South American segment of the Gondwanide orogen

The Gondwanide orogen in South America is widely distributed in the western region of Argentina and Chile, being parallel to the present-day N-S trending Andean chain north of 36°S latitude, overprinting pre-

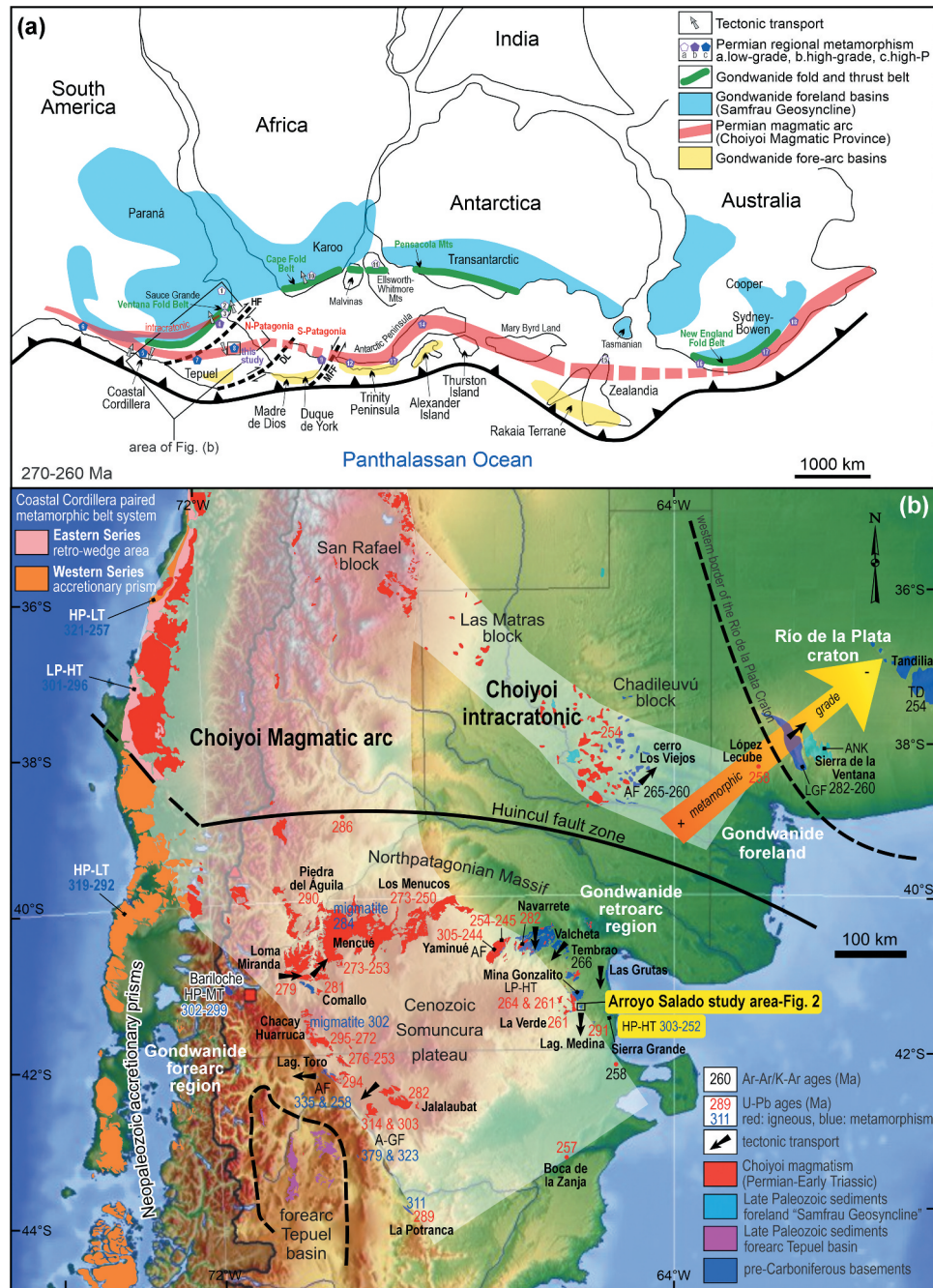


Figure 1. (a) Guadalupian tectonic setting of the southwestern Gondwana margin and palaeogeographic location of Patagonia, adapted from Lawver *et al.* (1998). Data of Permian regional metamorphism: 1. Río de la Plata Craton, telodigenesis: 254 Ma (Zalba *et al.* 2007). 2. Ventana, ankizone (NE region): 282–260 Ma (Varela *et al.* 1985; von Gosen *et al.* 1991). 4. Cerro Los Viejos, amphibolite facies: 265–260 Ma (Tickyj *et al.* 1997). 5. Coastal Cordillera, paired metamorphic belt: HP-LT (Western Series), 350–400°C/7–11 kbar, 319–292 Ma and LP-HT (Eastern Series), 3 kbar, 301–296 Ma (Martin *et al.* 1999; Willner *et al.* 2005, 2009). 6. Limón Verde, northern Chile: HP-HT, 660–720°C/13 ± 1 kbar, ~270 Ma (Lucassen *et al.* 1999). 7. Bariloche, high-P/high-T (11 kbar–650°C): 302 & 299 Ma (Oriolo *et al.* 2019). 8. Arroyo Salado, HP-amphibolite facies: 303–252 Ma (this study). 9. Tierra del Fuego, high-amphibolite/granulite facies (730–770°C/2–3 kbar): 268 Ma (Hervé *et al.* 2010). 10. South Africa, low-greenschist facies; 350°C/2.5 kbar (S) to 210°C/~1.5 kbar (N): 255–253 Ma (Blewett and Phillips 2016; Blewett *et al.* 2019). 11. Ellsworth Mts, burial-laumontite facies: Permian, *sl* (Castle and Craddock 1975). 12. Eastern Graham Land, amphibolite facies (588°C/7.4 kbar–735°C/6.4 kbar): c. 280 & 258 Ma. 13. Horseshoe Island, high-grade: c. 270 Ma. 14. Mount Charity-Orion massif, amphibolite facies (677°C/4.6 kbar): 259–257 Ma (12–14: Wendt *et al.* 2008 and references therein). 15. Brook Street Terrane: prehnite-pumpellyite to greenschist facies: Late Permian, *sl*. 16. Nambucca Block, Eastern Australia, high-T/low-P: 300–290 Ma (Shaanan *et al.* 2014). 17. Wandilla Province, Coastal Sub-Province (Australia), high-T/low-P: 275–270 Ma. 18. Connors-Auburn sub-provinces, high-T/low-P: 300–290 Ma (15–18: Jessop *et al.* 2020). HF: Huincul Fault zone; DL: Deseado Lineament; MFF: Magallanes-Fagnano Fault. (b) Location of the Arroyo Salado study area in northern Patagonia's late Palaeozoic geodynamic setting. See references for the geochronological data in Table S5 of the SOM. TD: telodigenesis, ANK: ankizone, LGF: low-greenschist facies, AF: amphibolite facies.

Carboniferous rocks with brittle deformation (Figure 1(b)). According to Sato *et al.* (2015), three stages characterize the arc magmatism of the Choiyoi Province at these latitudes: (1) pre-Choiyoi orogenic (>286 Ma), (2) the main Choiyoi (286–247 Ma), and (3) post-Choiyoi extension-related (<247 Ma). This magmatic evolution is intimately associated with the Early Permian San Rafael orogenic phase at the base, which causes the folding and brittle thrusting without metamorphism of pre-Permian rocks, and the Triassic Huarpica extensional phase towards the top (e.g. Kleiman and Japas 2009; Sato *et al.* 2015).

South of 36°S, the Gondwanide orogen has an east-southeastward shift and expansion, spreading towards two extensive regions separated by the Huincul Fault zone: the northern area, encompassing the Las Matras Block, the Chadileuvú Block, and the Sierra de la Ventana; and the southern area in central-north Patagonia (Figure 1(b)). In the former, the Choiyoi magmatism reaches the SW border of the Río de la Plata Craton at López Lecube, and is also recognized in the subsurface, as part of the pre-rift rocks covered by the syn-rift sedimentary fills of the Late Triassic-Early Jurassic basins (Llambias *et al.* 2003 and references therein). The Permian deformation is brittle-ductile to ductile and occurs along with low-to-high grade metamorphism, thus involving deeper crustal levels than rocks north of 36°S. Therefore, establishing a strict correlation with the San Rafael phase is unlikely. Key localities with pre-Carboniferous basement rocks extend along a NW-SE striking belt of about 500 km long and 300 km wide, encompassing the SW border of the Río de la Plata Craton and bounded by the Huincul Fault zone to the south (Figure 1(b)). Cratonward, from Cerro Los Viejos to Sierra de la Ventana, the orogen records a Permian NE-verging folding and thrusting of Palaeozoic strata, where the Sauce Grande foreland basin developed contemporaneously. Folding and thrusting are accompanied by a dextral component of strike-slip deformation, thus documenting a bulk dextral transpressional regime for the belt (Cobbold *et al.* 1991; Ballivián Justiniano *et al.* 2023). In the Sierra de la Ventana fold-and-thrust belt, the metamorphic grade involving different structural levels increases towards the southwest, varying from anchizone with brittle deformation in the northeastern part to low-greenschist facies and brittle-ductile deformation in the southwestern part (von Gosen *et al.* 1991; López-Gamundí and Rossello 1998). Further southwest, amphibolite facies metamorphism and ductile deformation are documented at Cerro Los Viejos (Tickyj *et al.* 1997; Figure 1(b)). Ar-Ar and K-Ar ages of metamorphism-deformation are in the range of 282–260 Ma (Varela *et al.* 1985; von Gosen *et al.* 1991) for Sierra de la

Ventana, and 265–260 Ma for Cerro Los Viejos (Tickyj *et al.* 1997). In addition, the Neoproterozoic-Early Palaeozoic sedimentary cover of the Río de la Plata Craton records far-field Gondwanide telodiagenesis at 254 ± 7 Ma (K-Ar alunite, Zalba *et al.* 2007).

In central-northern Patagonia (39°–44°S), the Gondwanide tectono-metamorphic event and associated Choiyoi magmatism have a regional distribution along a NW-SE trending 400 km wide belt bounded by the Huincul Fault zone to the north and the Late Palaeozoic forearc Tepuel Basin to the southwest. Petrochronologic, structural, and stratigraphic evidence indicates that the Gondwanide orogeny represents the second event affecting the pre-Carboniferous igneous-metamorphic basement of this region after widespread Early- to Middle Palaeozoic orogenic processes (e.g. Llambias *et al.* 2002; Basei *et al.* 2002; von Gosen 2002, 2003, 2009; Gregori *et al.* 2008; Marcos *et al.* 2018; Renda *et al.* 2021; Oriolo *et al.* 2023). Permian deformation and metamorphism (Giacosa 1994, 2001) reworked pre-Carboniferous NW-SE-trending basement fabrics formed during the Ordovician Transpatagonian orogeny (González *et al.* 2021). Pre- and post-orogenic granitoids are interpreted concerning the Permian deformation (González and Giacosa 2021).

S- to SW-directed late Palaeozoic thrusting along mylonitic belts affected the basement in localities of central-northern Patagonia such as Yaminué-Valcheta (Figure 1(b), Chernicoff and Caminos 1996; von Gosen 2003; Greco *et al.* 2017), Las Grutas, and Mina Gonzalito areas (Giacosa 1994, 2001; von Gosen 2002; González *et al.* 2008a, 2008b). On a regional scale, thrusting and mylonitic belts are comparable to the Cerro de Los Viejos-Sierra de la Ventana fold-and-thrust belt but with an opposite structural vergence. Transpression occurred to the north and south of the Huincul Fault zone, thus leading to the double-verging character of the Gondwanide orogeny. Within this structural framework, this fault zone is a cluster of parallel faults with prolonged motion along which the central-northern Patagonian crust was relatively displaced from Gondwana South America (e.g. von Gosen 2002; Gregori *et al.* 2008).

Geotectonic models for the Gondwanide orogen

Two geotectonic settings have been proposed for the late Palaeozoic Gondwanide orogen along the Panthalassan margin of Patagonia. In the first scenario, the orogeny is the result of plate convergence developing a subduction zone with a wide Andean-type magmatic arc to the southwest of the Sierra de la Ventana, including its fore-arc region and the retroarc foreland

(Dalziel and Grunow 1992; López-Gamundí and Rossello 1998), documenting bulk dextral transpression (Cobbold *et al.* 1991; Ballivián Justiniano *et al.* 2023). The development of an advancing orogen with crustal shortening resulted from slab shallowing, with the subsequent maturation and stabilization of the Patagonian continental crust due to widespread magmatism and crustal thickening by progressively increase in the reworking of pre-Carboniferous crustal components. This non-collisional model favours an in situ middle-late Palaeozoic crustal growth of Patagonia during changing dynamics of an accretionary orogen (Marcos *et al.* 2018, 2020; Suárez *et al.* 2019; Oriolo *et al.* 2019, 2023; Renda *et al.* 2021).

The second tectonic scenario proposes the collision of Patagonia as a separate terrane with the SW Gondwana border (Ramos 1984; von Gosen 2002, 2003, 2009; Pankhurst *et al.* 2006). This model assumes a subduction zone dipping southwestwards under Patagonia (Ramos 1984, 2008) to account for the late Palaeozoic subduction-related and syn-collisional magmatism (Pankhurst *et al.* 2006) recorded along the northern margin of this block, together with the progressive ocean closing and final amalgamation of the Patagonia continental block against Gondwana. According to this model, the suture along the Huincul Fault zone cannot be directly observed because younger sediments cover the area (Figure 1(b); e.g. Ramos 1984). The relatively low metamorphic grade in the foreland region argues against the collision of a major crustal block. Alternatively, very-low- to low-grade metamorphism and deformation in the foreland were interpreted as the result of an intraplate reactivation of the boundary between the Río de la Plata Craton and the Sierra de la Ventana basement (Christiansen *et al.* 2021). Though possible, regional evidence rather favours a wide Andean-type belt with a retroarc compression more than a continental collision (Trouw and de Wit 1999; Cawood 2005; Oriolo *et al.* 2023). Furthermore, palaeomagnetic and palaeogeographic reconstructions refute rather than confirm Patagonia as an allochthonous block (e.g. Rapalini 1998; López-Gamundí and Rossello 1998).

Geologic framework of the study area

The basement in the Arroyo Salado study area is the Mina Gonzalito Metamorphic Complex (MGMC), consisting of alternating schist, paragneiss, amphibolite, and dolomitic marble beds without migmatite intercalations. A mean $^{87}\text{Sr}/^{86}\text{Sr}$ value of 0.707354 ± 0.000113 of marbles indicates a Middle Cambrian sedimentation age for the calcareous protolith (Varela *et al.* 2014). A granitic orthogneiss of possible Palaeozoic age containing

inclusions of schists is also intercalated in the high-grade rock succession (Figure 2).

The complex underwent a polyphase tectono-metamorphic evolution separated into at least two distinct events (Giacosa 1994, 2001; von Gosen 2003). According to U-Pb detrital zircon data from the Mina Gonzalito area, located further northwest of the study area (Figure 1(b)), the meta-clastic protolith deposition is also Cambrian, while high-grade metamorphism and ductile deformation occurred in the Ordovician (Pankhurst *et al.* 2006; Varela *et al.* 2011; Greco *et al.* 2014), thus documenting the first event forming the NW-SE fabric on the complex during the Transpatagonian orogeny (González *et al.* 2018; González and Giacosa 2021).

The structures of the second event are the El Jagüelito ductile shear zone and the Arroyo Salado antiform, which overprint previous fabrics (Giacosa 1994, 2001, Figure 2). The shear zone juxtaposed the basement of the MGMC against the Peñas Blancas Granite, containing septums of hornfels, phyllites, and schists of the El Jagüelito Formation to the west (Giacosa 1994, 2001; von Gosen 2003). Based on the Cambrian sedimentation age and the Ordovician tectono-metamorphic evolution (González *et al.* 2018), the El Jagüelito Formation has been considered the low- to medium-grade metamorphic equivalent of the high-grade MGMC (Giacosa 1994).

According to Giacosa (2001), the mylonitic foliation is NW-SE- to NNW-SSE-trending with moderate dips towards the NE-ESE, and the mylonitic lineation is sub-horizontal to gently plunging to the N-NE. Kinematic indicators point to right-lateral reverse shearing. Based on primary stratigraphic features and structural data, Giacosa (1994, 2001) suggested that ductile shearing and the Arroyo Salado antiform development likely occurred during the late Palaeozoic Gondwanide orogeny during ~NE-SW compression associated with dextral transpression, overprinting the Ordovician fabric. The post-Ordovician age of ductile shearing agrees with the intrusive feature of the Peñas Blancas Granite into the Cambrian El Jagüelito Formation and their U-Pb zircon 471 ± 2.8 Ma crystallization age (García *et al.* 2014). TIMS U-Pb zircon and Rb-Sr data further point to a Permian age of the second tectono-metamorphic event regionally affecting the MGMC (Basei *et al.* 2005; Varela *et al.* 2011).

Analytical methods and samples

We carried out field mapping and mesoscopic structural and metamorphic analysis in basement exposures along the Arroyo Salado Creek area in the North Patagonian Massif (Figure 1(b)). We collected a set of samples for

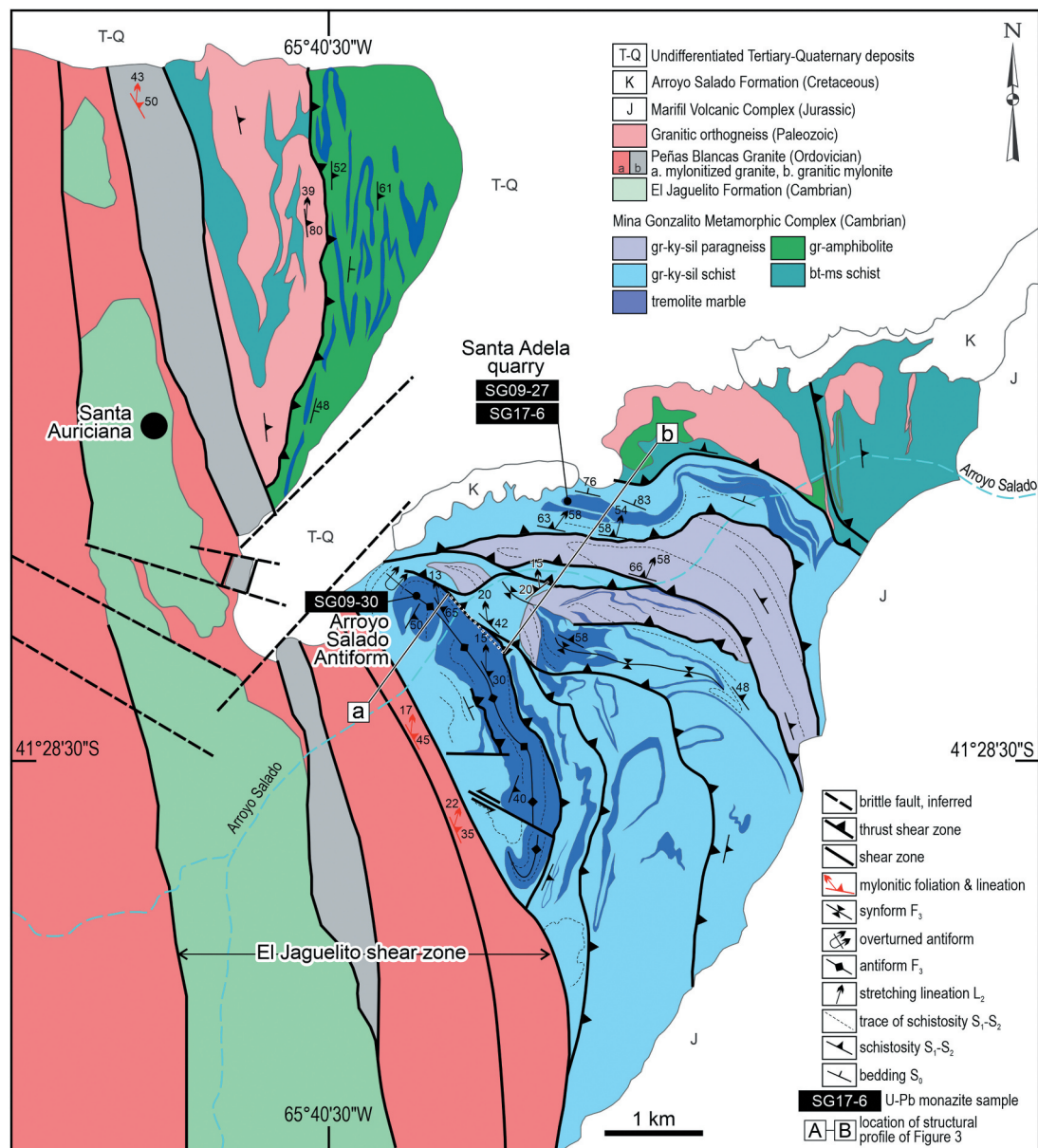


Figure 2. The geological map of the Mina Gonzalito Metamorphic Complex in the Arroyo Salado area is based on a visual interpretation of satellite images and was checked during our fieldwork. Locations of the studied samples and the structural profile (A) of Figure 3 are depicted.

microstructural, geochronologic, and thermobarometric constraints. Electron probe microanalyses (EPMA) of garnet, plagioclase, white mica, and biotite, used for conventional thermobarometry and multivariant equilibrium, were applied in two samples of schists (SG09–27 and SG09–30) to quantify pressure-temperature metamorphic conditions. Conventional pressure estimations were obtained with the garnet-biotite-muscovite-plagioclase barometer (Wu 2015), whereas temperature was calculated using a garnet-biotite thermometer (Holdaway 2000). A minimum error of $\pm 50^{\circ}\text{C}$ and ± 1 kbar has to be considered for each equilibrium calculation. Likewise, the TWQ software package (Berman 1991) was employed for

further P-T calculations, using solid solution models of Berman and Aranovich (1996), Berman (2007), Fuhrman and Lindsley (1988), and Chatterjee and Froese (1975) for garnet, biotite, plagioclase, and muscovite, respectively. The H_2O activity used was 1.

We also identified and located monazites by SEM-based automated mineralogy of three schist samples (SG09–27, SG09–30, SG17–06) at the TU Bergakademie Freiberg, Germany. Electron probe microanalysis was used for Th-U-Pb dating and to determine the chemical composition of monazites using a JEOL JXA 8530F at the Helmholtz-Institut Freiberg für Ressourcentechnologie, Freiberg, Germany. Sample descriptions, laboratory

procedures, analytical conditions, and any other relevant information on EPMA, TWQ, and SEM-AM are available in Tables S1, S2, S3, S4, and S5 and Figures S1 and S2 of the Supplemental online material (SOM).

Results

Structure

The regional-scale structure is a thick-skinned fold and thrust belt formed by a series of NW-trending thrust sheets and duplexes, separated by major thrust shear zones (Figure 2). The schematic structural profile of Figure 3 summarizes the relationship of different structural elements for the Arroyo Salado study area. The sedimentary stratification among protoliths is preserved as a S_0 compositional banding of (meta-) pelites, grey-wackes, dolostones, and marlstones, now comprising biotite-white mica-garnet-kyanite-sillimanite-rutile schists, biotite-garnet-rutile \pm sillimanite paragneisses, tremolite-bearing dolomitic marbles, and garnet para-amphibolites (Figure 4(a,b)). A granitic orthogneiss lies parallel to S_0 ,

although the primary stratigraphic intrusive relationship of its protolith is debatable (Figure 2). It contains biotite-muscovite schist inclusions, sharing the metamorphic fabric of sedimentary protoliths.

Isoclinal F_1 folds and the associated S_1 axial plane schistosity, best recorded in the marble outcrops, affect the S_0 banding (Figure 4(c)). Where present, rods of columnar carbonates define the L_1 lineation, oriented oblique to S_0 planes but not intersecting them, and visible at the outcrop scale and hand sample (Figure 4(d)). S_1 is also preserved as relics into porphyroblasts from schists, amphibolites, and marbles, being detectable in hand specimens and microscopic scales (Figures 4(e) and 5). The metamorphic axial plane foliation S_2 is the penetrative macroscopic fabric element of the metamorphic pile related to tight-to-isoclinal folds F_2 (Figure 4(d,f)). The shape-preferred orientation on S_2 planes of micas and sillimanite in metapelites and tremolite in marbles defines the stretching lineation L_2 .

The orientation of the S_0 and S_1 - S_2 planes strikes mainly NW-SE with variable dip despite showing dominant low to moderate angles towards the NE. The

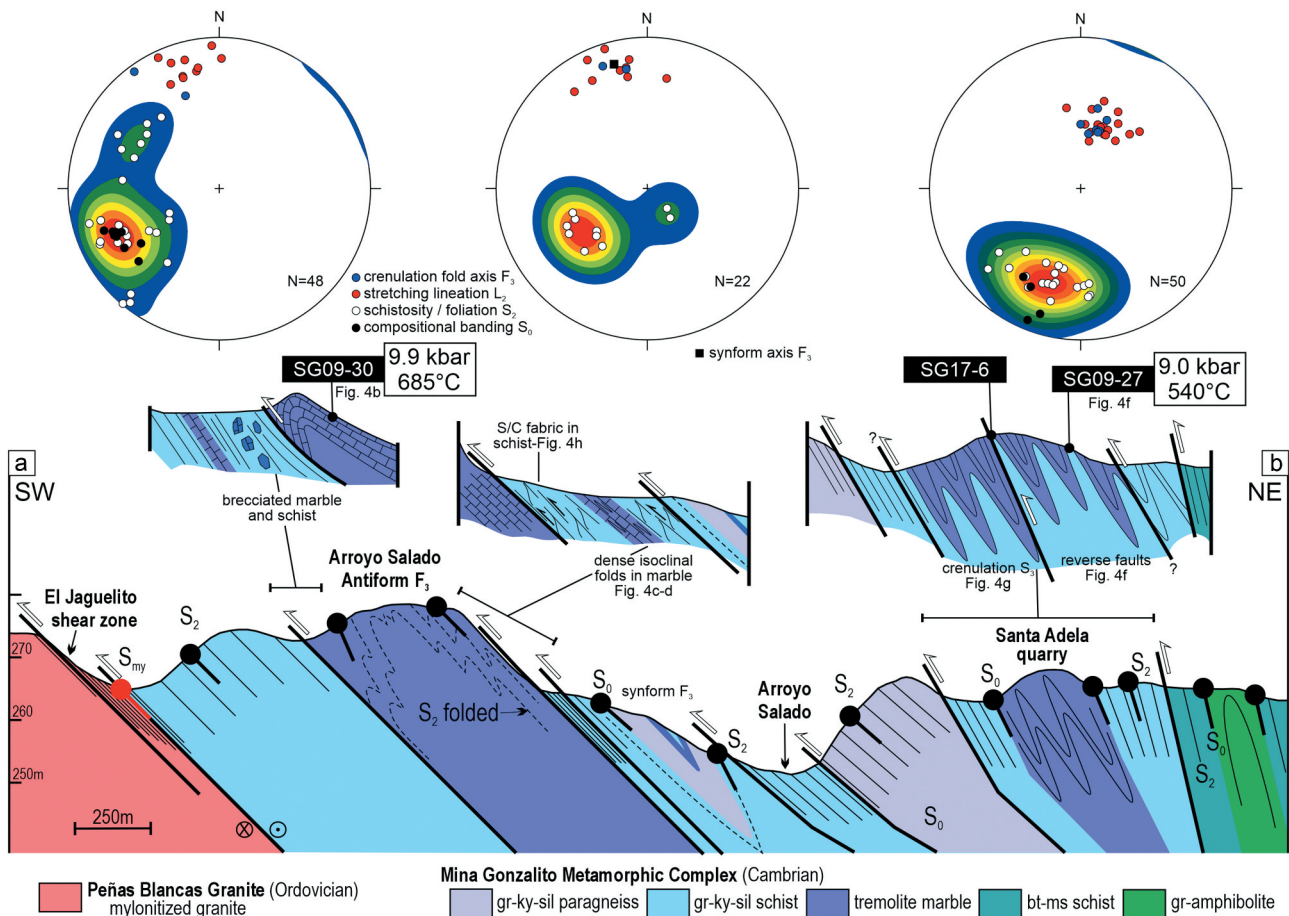


Figure 3. SW-NE structural profile showing the main structures mapped along the Arroyo Salado Creek area. Locations of the studied samples are also depicted. Stereo plots are lower hemisphere, equal-area projections of poles. Contour intervals at 2% per 1% area.

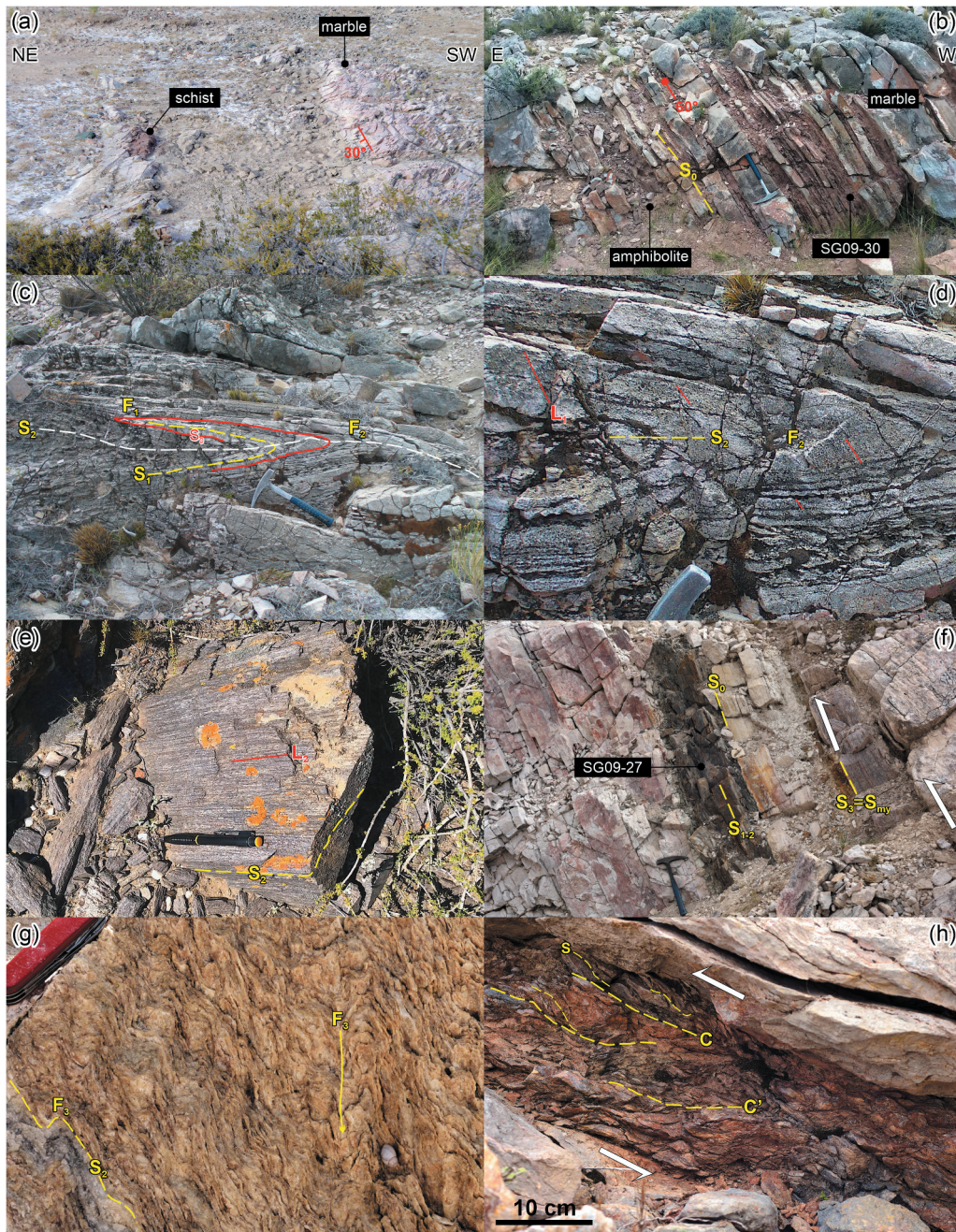


Figure 4. (a) Marble and schist intercalation in the Arroyo Salado Creek. (b) Northern part of the Arroyo Salado antiform (location in Fig. 3). Intercalation of schist, marble, and amphibolite beds marking the S_0 compositional banding. The schist bed SG09-30 sampled for petrochronology is also depicted. (c) Outcrop-scale internal structure of marbles evidenced by isoclinal F_1 refolded by tight F_2 folds. (d) Zoom in on the hinge zone of the F_2 tight fold in figure (c), showing rods of columnar carbonates defining the L_1 lineation. (e) Stretching lineation L_2 on S_2 schistosity planes in a paragneiss. (f) Tectono-metamorphic fabric of the schist bed SG09-27, which is intercalated among beds of dolomitic marble. (g) Crenulation centimetre-scale folds F_3 are shown in marbles. The penknife is 10 cm long. (h) S-C and C' fabric in a schist bed intercalated among beds of dolomitic marble, Santa Adela quarry (location in Figure 3).

stretching lineation L_2 exhibits sub-horizontal to gently plunge towards NNW-N in the west, becoming steeper towards NNE-NE in the east (Figure 3).

A regional-scale overturned antiform and synform F_3 refold all previous planar fabric elements, exhibiting a sub-horizontal NW-SE-trending axis (i.e. Arroyo

Salado antiform of Giacosa 1994). Another F_3 large-scale fold outlines the internal structure of a duplex containing a paragneiss sheet (Figure 2). Parasitic crenulation folds F_3 develop along the contacts between schist and marble, exhibiting parallel axes to the main folds defining the crenulation lineation L_3 (Figure 4(g)).

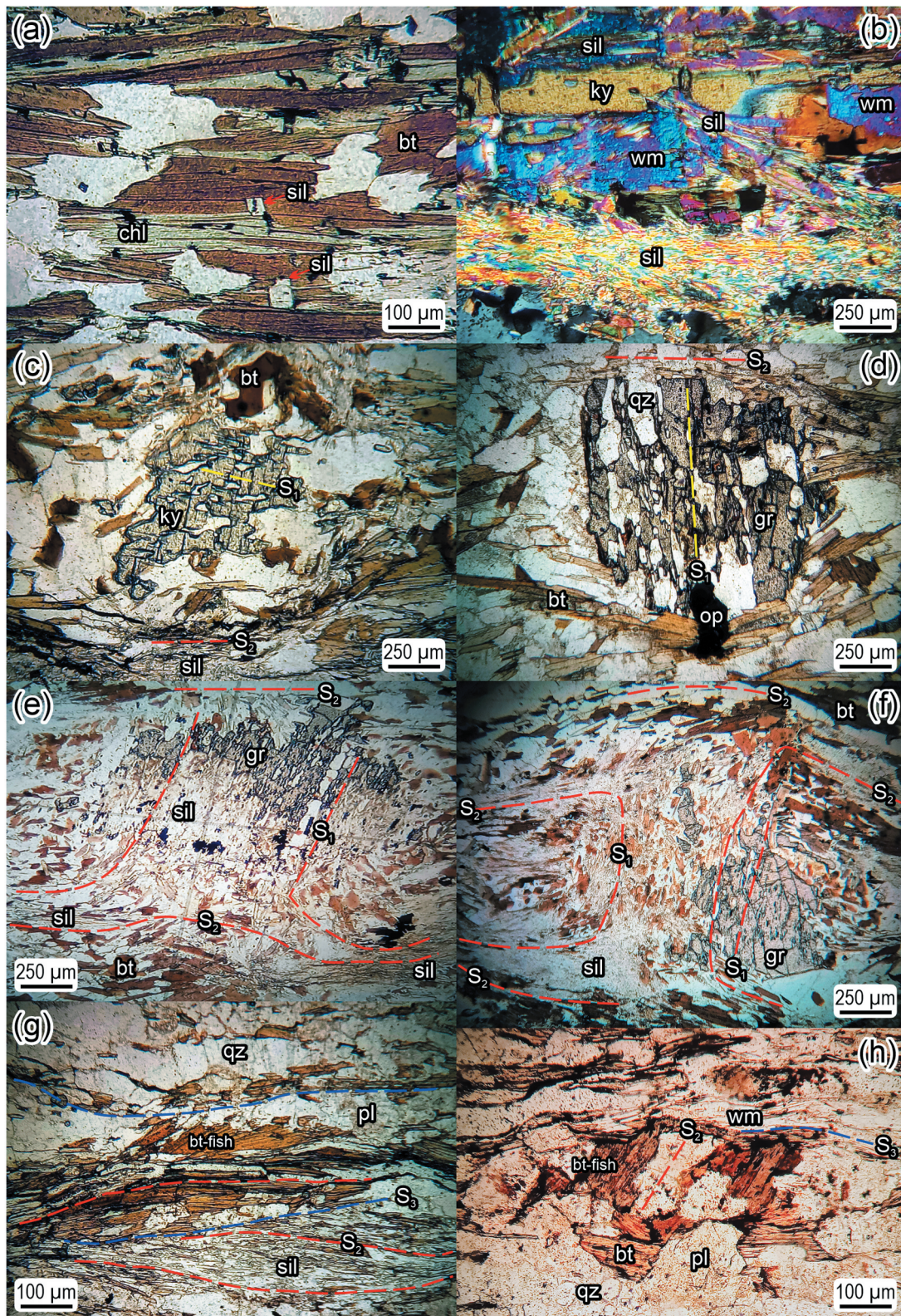


Figure 5. Photomicrographs from thin sections of schists (a-f) and mylonitic paragneiss (g-h) parallel and crossed polarizers. Details in the text. (a) Chlorite lamellae intergrowth in biotite. The chlorite-biotite pair is prograde because it is overprinted by sillimanite (basal sections), a higher-temperature mineral. (b) Sillimanite replacement on the white mica-kyanite porphyroblasts. (c) Intertectonic porphyroblast of kyanite with internal S_1 foliation surrounded by the S_2 schistosity of the matrix. (d) Intertectonic porphyroblast of garnet with S_1 internal and S_2 matrix schistosity. (e-f) Millipede microstructure around garnets replaced by sillimanite. S_1 - S_2 schistosity deflects in opposite directions. The inclusions correspond to S_1 and the matrix to S_2 . (g-h) Sillimanite prisms along the micro-shear bands S_3 developed parallel to S_2 . S_3 surrounds Group 1 (g) and Group 4 (h) biotite fishes (e.g. ten Grotenhuis *et al.* 2003). qz: quartz, pl: plagioclase, op: opaque, wm: white mica, chl: chlorite, bt: biotite, gr: garnet, ky: kyanite, sil: sillimanite.

High-angle ductile to brittle-ductile shear zones are the major thrusts of the fold and thrust belt associated with the F_3 folds forming thrust sheets and duplexes. The thrusts increased their angle of inclination towards the east from nearly 45° to 83° , along with the steepening of L_2 (Figure 3). A mylonitic foliation S_3 related to thrusts developed essentially parallel along the bedding contacts and also S_2 planes, acting as S_3 shear planes which seem to be associated with flexural slip between competent and incompetent layers (Figure 4(f)). The S_3 planes show a mylonitic lineation parallel to stretching lineation L_2 . Associated kinematic indicators (e.g. porphyroclasts and S-C shear bands, Figure 4(h)) show a top-to-the-S and SW ductile to brittle-ductile thrusting. Late fracturing with breccia and fault gouge development cross-cut all previous metamorphic fabrics parallel to bedding planes.

Metamorphism

We focus our metamorphic mineral assemblages and microstructure description on schists and paragneisses because they are the most widespread rock types, particularly for interpreting metamorphic conditions. In the case of marbles and amphibolites (synthesis in Table S1 of SOM), no significant differences in meso- and microstructures are observed, indicating that they record the same metamorphic evolution of metapelites (González *et al.* in prep.).

The schists record chlorite lamellae intergrowth with biotite, associated with quartz + plagioclase (zoned) + tourmaline + white mica + prismatic rutile + fibrolite/prismatic sillimanite. This association defines the S_2 schistosity surrounding post- S_1 and pre- to syn- S_2 white mica and kyanite porphyroblast intergrowths. Kyanite shows slightly rotated trails of S_1 quartz inclusions. Kyanite and sillimanite replace chlorite-biotite intergrowth along S_2 planes. Sillimanite replaces kyanite and white mica pseudomorphically or in rims (Figure 5(a–c)).

Intertectonic garnet poikiloblasts (post- S_1 /pre- to syn- S_2) surrounded by the S_2 schistosity are also common but are not in contact with kyanite. Three types of inclusion trails are observed: straight obliquely oriented, curved spiral-shaped to sigmoidal, or millipede S_1 inclusions trails of quartz, biotite, and opaque minerals. Sillimanite also pseudomorphically replaces garnet (Figure 5(d–f)).

Paragneisses are the coarse-grained counterparts of the schists, recording almost the same mineral assemblage and microstructures but lacking kyanite and tourmaline. Submicroscopic fibrolite needles are present parallel to the S_2 schistosity. The quartz + plagioclase + microcline association defines the granoblastic microstructure in microlithons. Paragneisses best record

micro-shear bands S_3 developed parallel to S_2 , crenulating micas or forming some biotite-fish porphyroclasts. Sillimanite prisms are commonly parallel to the S_2 - S_3 planes (Figure 5(g–h)).

Mineral chemistry and thermobarometry

In sample SG09–27, garnet porphyroblasts show significant core-to-rim compositional variations, except for spessartine ($Mn/(Fe_T + Mn + Mg + Ca)$) contents, which remain nearly homogeneous at ca. 21–24%. Grossular ($Ca/(Fe_T + Mn + Mg + Ca)$) and pyrope ($Mg/(Fe_T + Mn + Mg + Ca)$) in garnet cores are characterized by ca. 17–20 and 5–7%, respectively (Fig. S1 of SOM). In contrast, rims show respective grossular and pyrope contents of ca. 7–9 and 12–13%. Almandine ($Fe_T/(Fe_T + Mn + Mg + Ca)$) only depicts a slight increase from ca. 53% to 57% towards rims. On the other hand, no chemical differences are recorded in matrix biotite S_2 - S_3 and pre- S_2 biotite fish. X_{Mg} ($Mg/(Mg + Fe_T + Ti + Al^{VI})$) is generally at ca. 0.44–0.47, with ^{IV}Al of 1.23–1.26 apfu and X_{Ti} ($Ti/(Mg + Fe_T + Ti + Al^{VI})$) of 0.03–0.04. Only one crystal, which shows no apparent microstructural differences with further analysed biotites, offers a slightly different composition characterized by X_{Mg} of 0.51–0.52, ^{IV}Al of 1.24–1.25 apfu, and X_{Ti} of 0.05. White mica compositions in the matrix along S_2 are relatively homogeneous, with Si and Al^T of ca. 3.12–3.25 apfu and 2.43–2.72 apfu. Syn- S_2 plagioclase crystals are slightly zoned of oligoclase composition, ranging in anorthite ($Ca/(Ca + Na + K)$) contents of ca. 16–24%. Table S2 of SOM summarizes all the mineral chemistry used in P-T calculations.

Zonation patterns are also observed in garnet porphyroblasts of sample SG09–30, though they show compositional differences. Spessartine molar contents vary from ca. 8% to 16% from cores to rims, whereas no systematic pattern is observed for pyrope, which shows a proportion in the ca. 8–12% range. Grossular decreases from ca. 13% to 6% in one garnet crystal, though it shows a nearly homogeneous composition of ca. 12–13% in a second porphyroblast (Fig. S1 of SOM). Likewise, a somewhat irregular zonation pattern is evident in almandine, varying mainly between ca. 16% and 22%. Similarly to sample SG09–27, biotite, white mica, and plagioclase compositions are homogeneous along S_2 . In the case of biotite, X_{Mg} of ca. 0.33–0.36 corresponds to ^{IV}Al of 1.24–1.30 apfu and X_{Ti} of 0.05–0.06, whereas white mica exhibits Si and Al^T of ca. 3.11–3.20 apfu and 2.58–2.78 apfu. Plagioclases are also oligoclase, with the anorthite content ranging from 22% to 25%.

The chlorite-biotite-white mica-garnet-kyanite-sillimanite schist SG09–27 shows variations of P-T conditions from core to rim garnet growth. The three groups defined are controlled mainly by abrupt

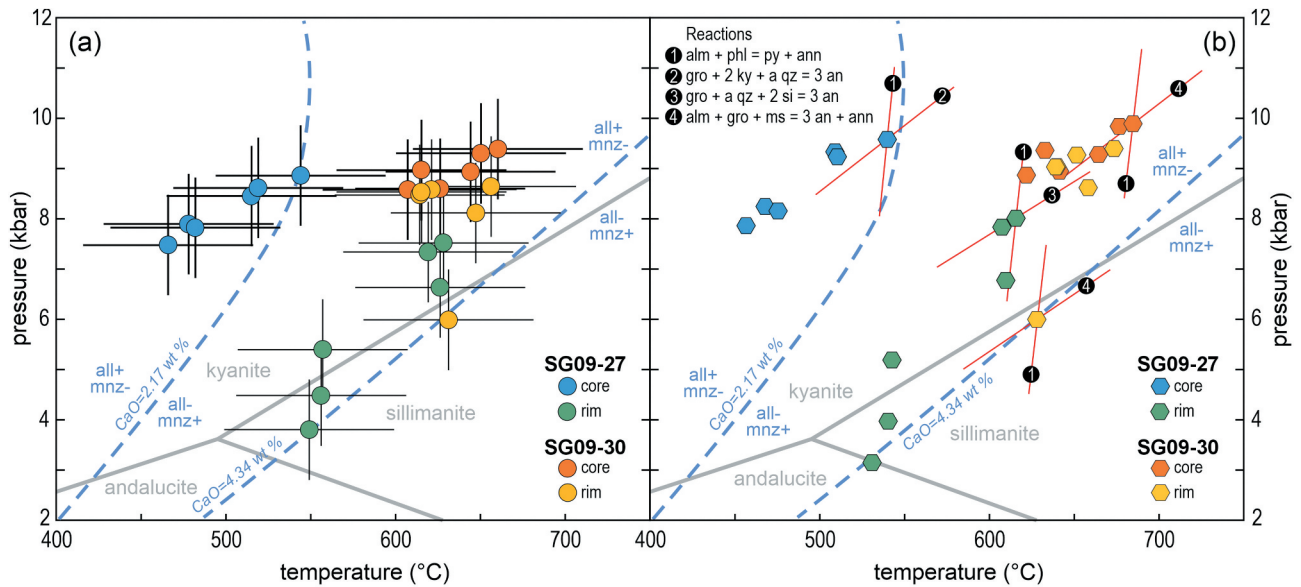


Figure 6. P-T paths based on (a) conventional thermobarometry and (b) multivariant equilibria (see text for further details). Table S3 of SOM depicts P-T data from both methodologies. For comparison, the monazite-allanite equilibrium (light-blue dashed line) curves published by Spear (2010) are projected, which were calculated for a metapelite with $\text{Al}_2\text{O}_3 = 16.57$ wt % and variable CaO contents (2.17 and 4.34 wt %). Mineral abbreviations: all: allanite, mnz: monazite, alm: almandine, phl: phlogopite, py: pyrope, ann: annite, gro: grossular, ky: kyanite, qz: quartz, an: anortite, si: sillimanite, ms: muscovite.

changes in the garnet, though they may be arbitrary. Cores increase progressively between 7.5–9.0 kbar and 460–540°C and rim compositions register a continuous retrogression from 7.5 to 6.6 kbar and 620–630°C to 5.4–3.8 kbar and 550–560°C (Figure 6(a)). TWQ parallel conventional estimations within errors computed as ± 1 kbar and $\pm 50^\circ\text{C}$. Under prograde conditions, garnet core compositions reached up to 9.6 kbar at 540°C, then retrogressive P-T conditions indicated by rim compositions from ca. 8.0 kbar and 616°C culminating within the sillimanite stability field (Figure 6(b), Table S3 of SOM).

Biotite-white mica-garnet \pm sillimanite schist SG09-30 has two temperature data clusters around 610–625°C and 650–660°C for overall 8.5–9.4 kbar to both cores and rims. Although they do not record extensive P-T analytical differences within errors, core compositions register slightly higher pressure than rims (Figure 6(a)). A 6.0 kbar-630°C datum separated from clusters follows retrogression, entering the stability field of sillimanite. TWQ data also reproduce conventional estimations within errors. P-T data of core and rim compositions share the same prograde cluster from 8.9 kbar-622°C to peak P-T at 9.9 kbar-685°C for cores and then following retrogression up to 6.0 kbar and 632°C to rims (Figure 6(b), Table S3 of SOM).

Monazite chemistry and petrochronology

Backscattered electron images (BSE) data show that monazites are commonly oriented parallel to the S_2

schistosity in the matrix associated with white mica, biotite, quartz, and feldspars (Figure 7). Although some monazite crystals are homogeneous, complex and patchy zonation patterns are common, suggesting coupled dissolution-reprecipitation processes. Therefore, the crystal internal age distribution is random or follows their patchy zoning (Figure 7).

Monazite ages point mostly to Permian metamorphism and deformation (Figures 8 and 9(a); Figure S2 and Table S4 of SOM). Sample SG09-30 shows an age of 258 ± 3 Ma, though a minor population also yielded 289 ± 7 Ma. Similarly, for sample SG09-27, a main age of 271 ± 2 Ma was obtained along with a 303 ± 5 Ma age (Upper Pennsylvanian). For schist SG17-6, a single monazite data of 252 ± 6 Ma is further supported by the unimodal age distribution of individual monazite ages, pointing to the dominance of Lopingian ages, with subordinate Late Carboniferous to Early Permian contributions (Figure 8).

Key parameters of monazite chemistry also assess age groups. No significant intrasample differences are observed for Y_2O_3 and UO_2 contents, which are also roughly comparable among samples (Figure 9(b,c)).

On the other hand, the monazite-allanite equilibria (Spear 2010) allow for the evaluation of the petrochronologic significance of monazite ages in the physical conditions of the studied rocks (Figure 6) and, therefore, in p-T-t paths (see below discussion). In this

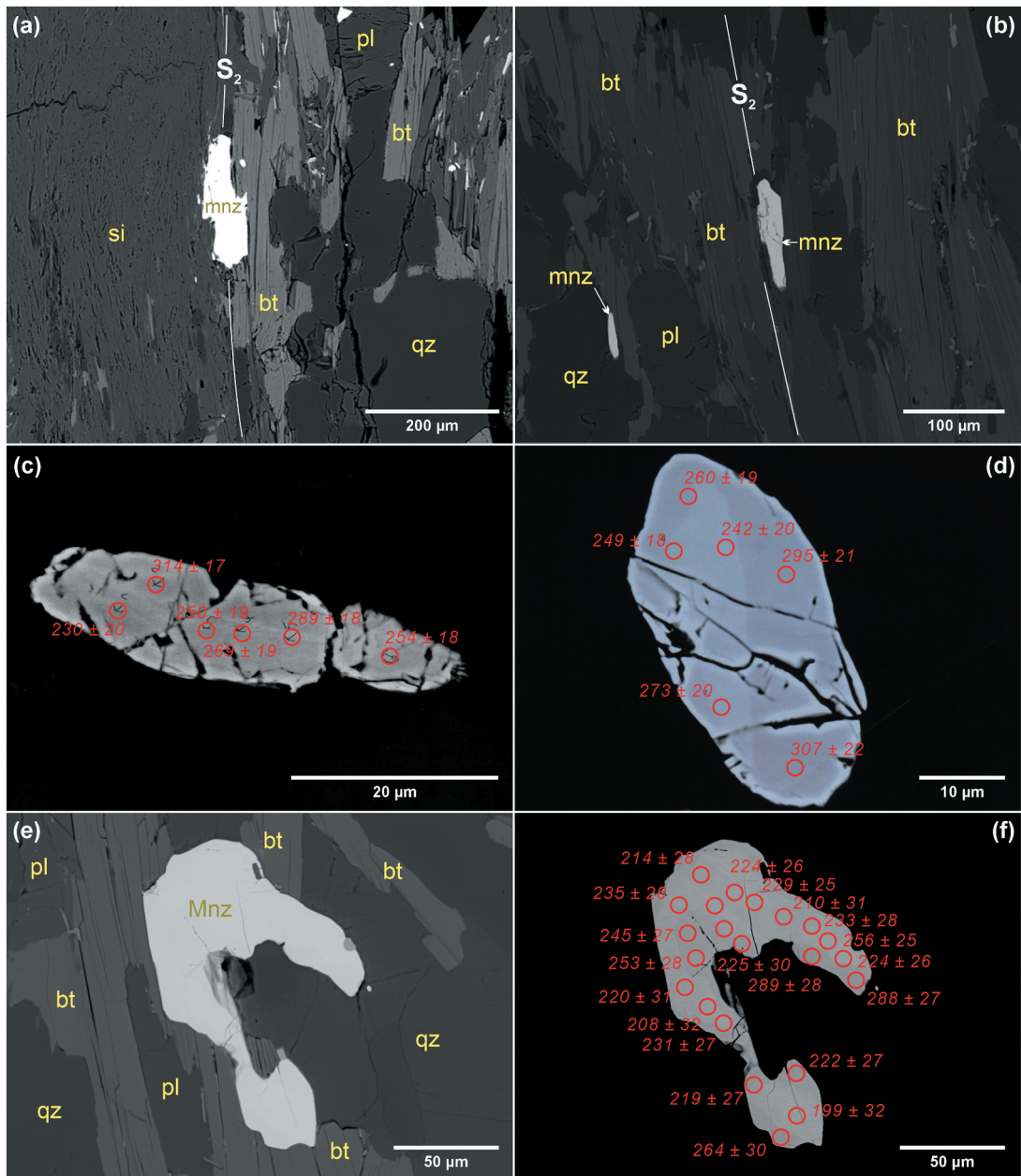


Figure 7. Backscattered electron images (BSE) of thin sections showing monazites commonly oriented parallel to the S_2 schistosity and single Th-U-Pb ages (Ma, 2σ error). (a, d) Sample SG09-27. (b, e, f) Sample SG17-6. (c) Sample SG09-30. Mineral abbreviations: qz: quartz, pl: plagioclase, bt: biotite, si: sillimanite, mnz: monazite.

context, Al_2O_3 and CaO are also particularly relevant in metapelites since they significantly affect the monazite-allanite equilibrium (Spear 2010). In SG09-27 and SG09-30, Al_2O_3 contents are 16.61 and 15.64 wt %, respectively, nearly equivalent to the value of 16.57 wt % modelled by Spear (2010). CaO is variable between them, exhibiting respective contents of 1.89 and 4.30 wt %.¹ Therefore, for SG09-27, the true equilibrium line may be slightly shifted towards lower-temperature, mainly due to the lower Ca contents

regarding the $CaO = 2.17$ wt % curve, indicating that monazite might have been stable already during part of the prograde stage and also during subsequent retrogression (Figure 6(a)). It also in line with the predicted monazite + garnet + kyanite/sillimanite equilibrium conditions (Spear 2010). In contrast, the relatively high CaO contents of SG09-30 close to the equilibrium line ($CaO = 4.34$ wt %, Figure 6(b)) suggest that monazite might have been stable first during late stages recorded by garnet rim conditions.

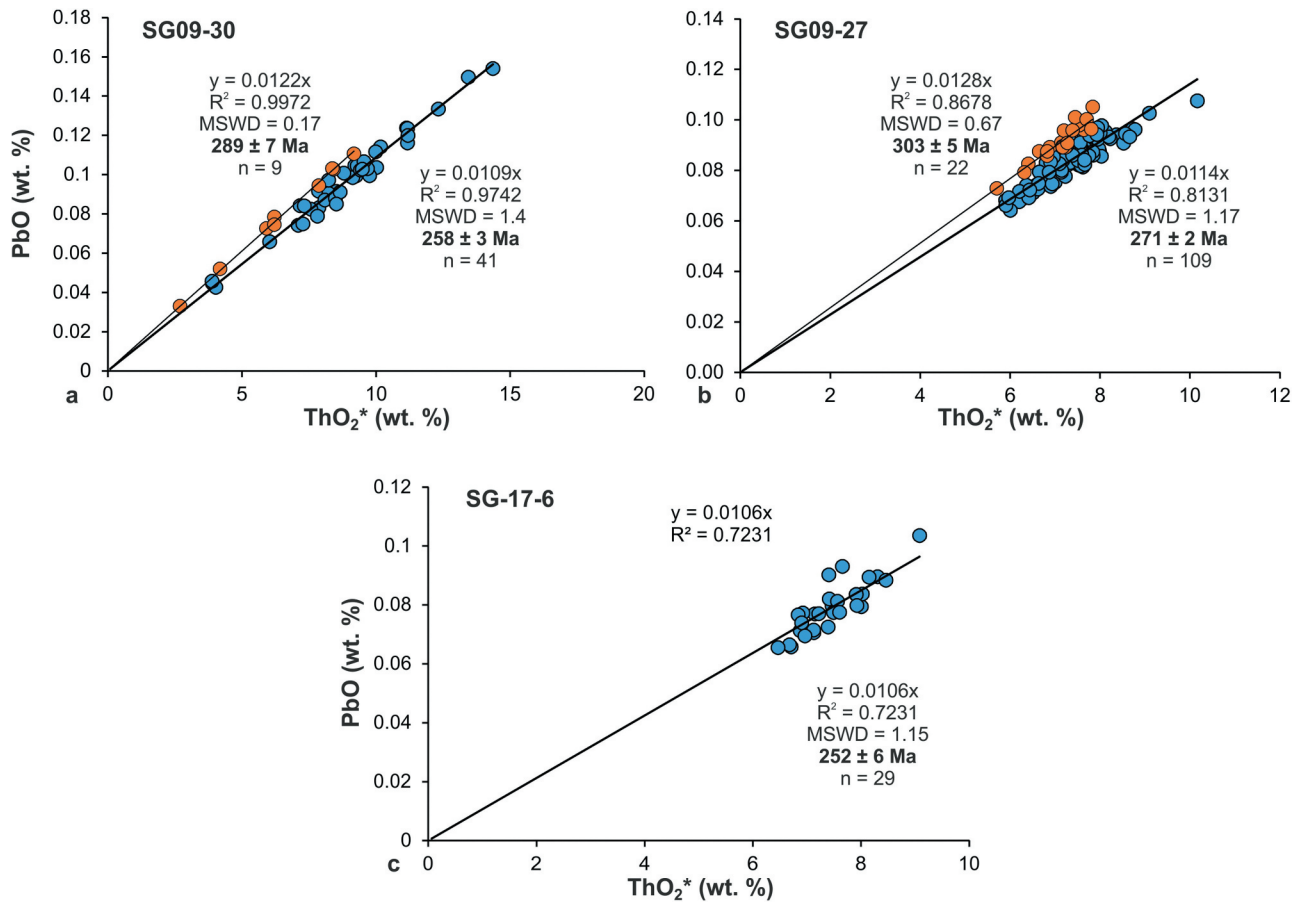


Figure 8. Th-U-Pb chemical model ages of monazite. Total ThO_2^* vs PbO (wt %) isochrones diagrams. ThO_2^* is $\text{ThO}_2 + \text{UO}_2$ equivalents expressed as ThO_2 . Regression lines with the coefficient of determination R^2 are forced through zero (Suzuki *et al.* 1994; Montel *et al.* 1996). Weighted average ages (Ma) with MSWD and minimal 2σ error are calculated from single analyses according to Ludwig (2001). Light blue and orange circles represent the different monazite age populations.

Discussion

The P-T-t path

Mineral assemblages and replacement microstructures, mineral chemistry and geothermobarometry, and Th-U-Pb monazite dating reveal typical features of a clockwise metamorphic evolution. Each sample has distinctive P-T-t paths reflecting three stages of continuously changing P-T conditions. Both schists studied share a relatively high-P prograde M_1 stage responsible for the inversion of the biotite and garnet isograds, albite-dominated plagioclase, the relatively Ca- and Mg-rich garnet cores, and Si-rich white mica. Intertectonic growth of garnet, kyanite, and white mica porphyroblasts marks peak-P conditions, although there is no microstructural evidence for kyanite growth together with the garnet core in SG09-27. However, both phases are replaced by sillimanite, suggesting a roughly contemporaneous nucleation. The elevated Na and Ca activities during the growth of high-Ca garnet (e.g. Lü *et al.*

2023), supported by the common presence of a sodic plagioclase core (Table S2 of SOM), may account for the lack of kyanite in SG09-30.

Peak-P conditions among samples are slightly diachronous. While the schist SG09-30 reached peak-P contemporaneous with T at high amphibolite facies, in the schist SG09-27, it developed under low amphibolite facies before peak-T and close to the blueschist-eclogite facies transitional field (Figure 10(a,b)). Conventional thermobarometry together with TWQ multiequilibria indicates garnet cores achieved peak P-T at ca. 9.9 kbar and 685°C for SG09-30, and the peak-P for SG09-27 was 9.0–9.6 kbar at ca. 540°C. Therefore, the M_1 stage was of rapid burial and distinctive heating under relatively low geothermal gradients of ~15 and 20°C/km for SG09-27 and SG09-30, respectively.

After the M_1 stage, evolution followed different paths in the two samples. The growth of garnet rims and biotite + white mica of the matrix subsequently replaced by sillimanite + rutile marks the M_2 retrograde stage in the schist SG09-30 (Figure 5(d-f)). It is

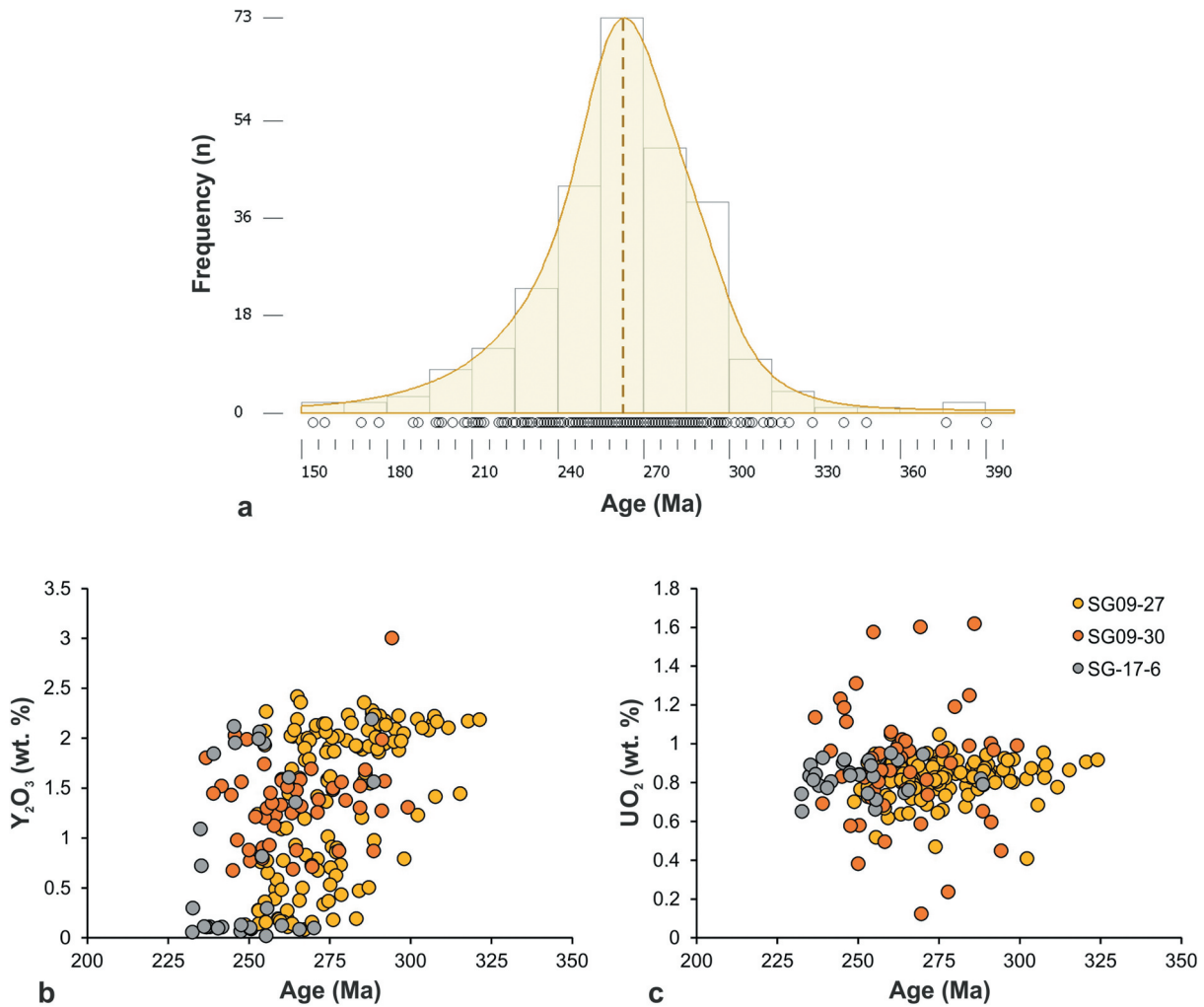


Figure 9. (a) Distribution of chemical Th-U-Pb monazite ages of the three analysed samples. (b-c) Mineral chemistry of samples. See details in text. Kernel density estimate curves and histograms plotted using DensityPlotter ($n = 271$; Vermeesch 2012).

characterized by a near isothermal decompression, as is indicated by $\sim 35^\circ\text{C}$ cooling in a range of ~ 2 kbar (up to ~ 8 kbar and 645°C), though some garnet rim compositions are parallel to the prograde path. This duality may account for the core-to-rim zoning of garnet porphyroblasts reflecting microchemical disequilibrium across the complex interplay of temperature, high-strain deformation, time, and the availability and mobility of intergranular fluids (e.g. Gaidies 2021; Dubosq *et al.* 2024). Afterward, following the same trend of isothermal decompression, a late M_3 stage recorded 6.0 kbar and 632°C within the stability field of sillimanite, though only one point yields a low P value following the near isothermal decompression path (Figure 10(b)). In this same regard, core-to-rim variations in garnets of SG09–30, particularly in Mn and, subordinately, Ca-Fe are subtle (Fig. S1 of SOM), and syn- S_3 sillimanite replacing syn- S_2 biotite and white

mica in the matrix documents the overall exhumation path (Figure 5(g,h), and SOM).

After the peak P , the schist SG09–27 records a stepped evolution characterized by two distinctive metamorphic stages. In addition to garnet rims + white-mica and biotite, sillimanite + rutile also replace kyanite porphyroblasts, marking the M_2 stage outlined by a loop of heating and decompression with a T climax ranging 616 – 627°C at ~ 8.0 kbar, then following a near isothermal ($<20^\circ$ cooling) decompression up to ~ 6.7 kbar (Figure 10(a)). Then, the M_3 stage is also of isothermal decompression, after about 550°C and a decrease in P from 5.5 to 3.0 kbar culminating within the sillimanite stability field. Therefore, both samples overall retrogressive M_2 – M_3 trends follow a Barrovian overprint under a kyanite-sillimanite geotherm ($\sim 30^\circ\text{C}/\text{km}$).

On the other hand, the continuously changing P – T data compared with monazite chemistry and monazite-allanite

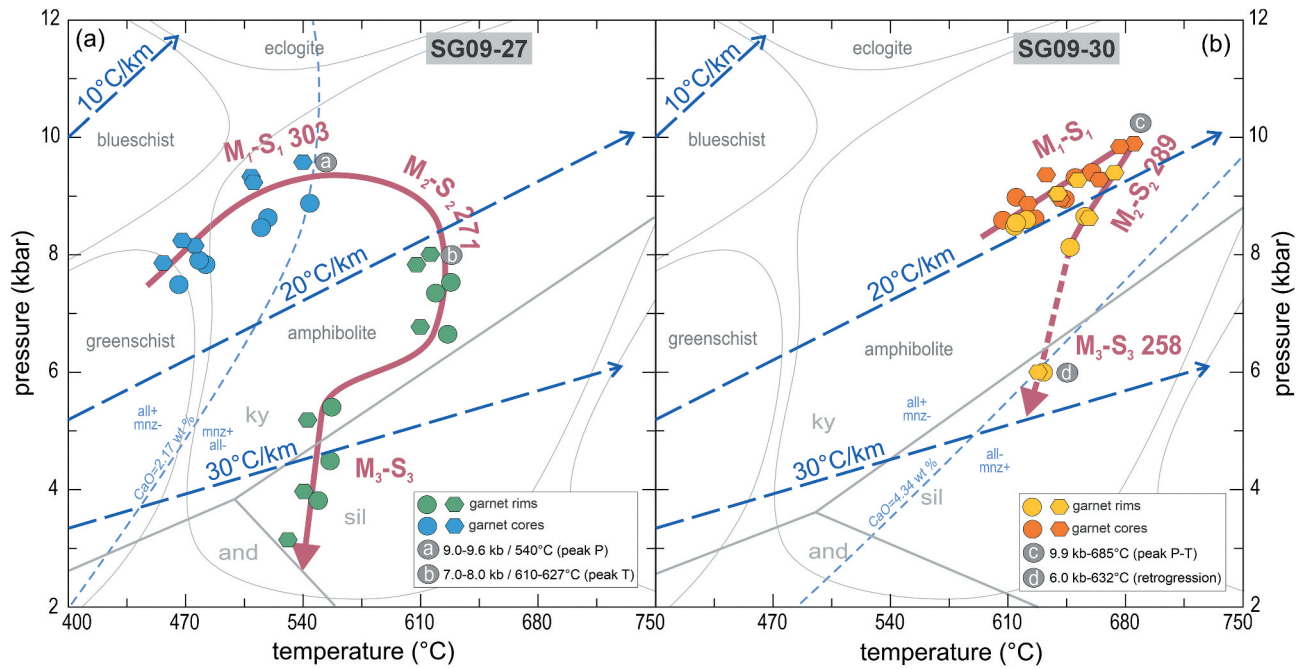


Figure 10. Clockwise P-T-t-D paths of the analysed schist samples. They are slightly diachronous. Monazite-allanite equilibrium (light-blue dashed line) based on Spear (2010) as in Figure 6. (a) Peak-P reached before peak-T, also describing a wide loop. (b) Simultaneous peak P-T. Only one point yields a low P value for retrogression (dashed line), and therefore the interpretation for the exhumation path is conservative. Evolutionary details in text.

equilibrium conditions (Spear 2010, Figure 6) resulted in a single metamorphic event, as recorded by the low intra- and intersample variability of Y_2O_3 and UO_2 contents (Figures 8 and 9). Microstructural evidence of coupled dissolution-precipitation processes may suggest long-term medium-to-high-grade metamorphic conditions favouring monazite growth during some tens of My, possibly due to the wide stability field of monazite in samples yielding meagre CaO contents. However, peak metamorphic conditions were slightly diachronous among samples reached during the M_1 and M_2 stages in SG09-30 and SG09-27, respectively. Therefore, the 303 ± 5 Ma secondary data of SG09-27 is interpreted as prograde monazite crystallization at the expense of allanite at peak-P during M_1 (9.6 kbar-540°C) in the Upper Pennsylvanian. The 271 ± 2 Ma age is explained as monazite crystallization during the T-peak of the M_2 stage in the Guadalupian, mid-Permian (Figure 10(a)), and possibly continuing along the retrograde stage towards M_3 .

For SG09-30, the 258 ± 3 Ma data is interpreted as the age of M_3 retrogression in the Lopingian, Late Permian. The minor monazite population of 289 ± 7 Ma may represent the earlier M_1 or M_2 stages in the Cisuralian, Early Permian, mainly related to peak P-T conditions (Figure 8). Growth of monazites from M_1 - M_2 to M_3 temperature conditions points to a fluid-induced, coupled dissolution-precipitation of pre-existing monazite (e.g. Zi *et al.* 2024 and references therein), leading to the

development of irregular internal crystal microstructures as evidenced by BSE imaging of similar chemical composition (Figure 7). On the other hand, the age of 252 ± 6 Ma from SG09-17 also supports the Lopingian, Late Permian M_3 metamorphic stage, due to the mylonitic fabric of the schist within a thrust shear zone (Figure 3). The SG09-17 schist is in line with the P-T paths of the samples mentioned above, in the fact of lacking significant differences in the succession of mineral assemblages and microstructural relationships (petrographic descriptions in the SOM) and in terms of monazite chemistry (Figures 8 and 9).

Integrating deformation in the P-T-t path

The thick-skinned fold-and-thrust belt of the MGMC is spatially and temporally related to the geometry and kinematics of the El Jagüelito ductile shear zone (Figures 2 and 3). The co-planar fabric arrangement of the deformation belt, evidenced by the relic S_0 bedding and S_1 planes, the ubiquitous S_2 schistosity, and the subsequent development of the S_3 mylonitic foliation, shows a dominant NW-SE strike with low to moderate dips, steepening towards the NE. Similarly, the stretching lineation L_2 parallel to the mylonitic lineation L_3 exhibits a sub-horizontal to gentle plunge towards NNW-N in the west, becoming steeper towards NNE-NE in the east (Figure 3). Kinematics of reverse shear zones show a top-

to-the-S and SW ductile to brittle-ductile thrusting of sheets and duplexes in the west and east, respectively (Figure 2). Thus, the southwestern sector close to the El Jagüelito shear zone has a localized predominance of dextral shearing. In contrast, the northeastward area has a dominant reverse component, as Giacosa (1994, 2001) also reported. Thus, our structural and kinematic data in the Arroyo Salado study area point to bulk-inclined transpression (Jones *et al.* 2004), with strain partitioning into strike-slip and contraction-dominated domains (e.g. Oriolo *et al.* 2019). Likewise, Giacosa (1994, 2001) interpreted the coeval development of El Jagüelito ductile shear zone and Arroyo Salado antiform due to ~NE-SW compressive regional stress field in a dextral transpressional regime (see above geotectonic models). In this context, shear zones and related S_3 might have thus resulted from the progressive crustal shortening and folding of metasedimentary sequences.

Linking the complex structural pattern in the clockwise P-T-t path further documents a single-phase progressive ductile event under continuously changing metamorphic conditions. The development of multiple coaxial structures, overprinting each other sequentially, characterizes progressive deformation (Fossen *et al.* 2018). Likewise, heterogeneous strain partitioning and localization in a transpressional setting usually explain single-phase progressive deformation (Fossen *et al.* 2013; Oriolo *et al.* 2023; Lardeaux 2024). Or else, disequilibrium microstructures (e.g. coronas, intertectonic, and millipede porphyroblasts, Figure 5(e-f)) indicate that metamorphic reactions did not complete under the ongoing deformation, tracking progressive foliation development relative to actively changing metamorphic conditions (Johnson 1999). Therefore, relatively rapid burial and heating into the deep crust led to the development of S_1 planes under regional high-P M_1 metamorphism under prograde conditions from upper greenschist to upper amphibolite facies. Then, the ubiquitous S_2 schistosity developed coevally with M_2 heating and peak conditions and possibly continued during the early decompression, which culminated with syn- M_3 development of the S_3 mylonitic foliation (Figure 10). Thus, the deformation belt evolved from a high-P/high-T prograde regional metamorphism during M_1 - S_1 / M_2 - S_2 to a more localized retrograde low-amphibolite facies dynamic metamorphism during M_3 - S_3 .

Consequently, kinematically active thrust shear zones can explain the slightly diachronous clockwise P-T-t-D evolution among samples assessed through the thrust sheets and duplexes. They also strengthen the temporal-spatial and kinematic relationship between the El Jagüelito shear zone and the thick-skinned fold and thrust belt of the MGMC. Thrust shear zones were

tectonic boundaries separating sheets of unlike P-T evolution and exhuming slightly different portions of the deep crust (e.g. Tenczer and Stüwe 2003). Metamorphic grade decreases isobarically near structurally upward over a distance of about 4000 m along the Arroyo Salado Creek (Figure 3). The sheet containing schist SG09–30 in the Arroyo Salado antiform close to the El Jagüelito shear zone is of relatively higher P-T than Santa Adela schist SG09–27 eastward (Figure 10). Subsequently, an increase in age with decreasing metamorphic grade can be explained by differential exhumation along a traverse section of the deformation belt (e.g. Oriolo *et al.* 2019, 2023). The horizontal T-gradient from west to east can thus be explained by the heat advection and relative diffusion rates during the belt exhumation (Sonder and Chamberlain 1992). Alternatively, the shear heating and more localized deformation adjacent to the El Jagüelito shear zone can correlate with relatively higher P-T of SG09–30 (e.g. Tenczer and Stüwe 2003). Thus, the right-lateral transpressive deformation and strain partitioning within the belt were critical in disturbing regional isograds due to stress overpressure and frictional heating.

We then speculate that the peculiar P-T-t-D evolution at peak metamorphic conditions might be associated with a relatively fast exhumation of the orogenic roots, which dominantly occurred during sheet and duplex stacking caused by the continuous underthrusting and consequent crustal thickening during the evolution of the Gondwanide orogen (Figure 11(a,b); e.g. Oriolo *et al.* 2019, 2023; Marcos *et al.* 2020, 2023). Furthermore, post-metamorphic fluid infiltration, evidenced by scarce post- M_3 - S_3 chlorite + sericite-muscovite replacement over biotite + kyanite (Table S1 of SOM), was likely of minor importance due to the preservation of the high-P relics during exhumation. This rather dry condition can also be linked to the relatively fast extrusion of the deformation belt. A volume of rock that is rapidly exhumed from depth, perhaps in response to unroofing via erosion, may account for large-magnitude isothermal decompression, transporting heat to near-surface depths, reflecting that either exhumation rates were more rapid than those of heat transfer (thermal relaxation) or there was a considerable lag time (>10 My) between crustal thickening (deep burial) and the initiation of denudation (e.g. Whitney *et al.* 2004; Likhonov 2020; Peillod *et al.* 2024).

In sum, the overall information recovered by P-T-t-D paths shows that the regional clockwise single-phase progressive deformation and high- to medium-P amphibolite facies metamorphic event of the MGMC span on the order of around 50 My, developed almost entirely within Permian transpressional regime linked

with the Gondwanide orogeny. However, considering the regional geologic knowledge of the complex, it developed during a polyphase evolution resulting from the Ordovician Transpatagonian and Neopaleozoic Gondwanide events (González *et al.* 2021). Thus, the high-P stage has given the rocks their most robust character and would have reset the Ordovician ages of metamorphism-deformation. Or else, since a complete reset to a previous fabric is sometimes unlikely, the protoliths in the Arroyo Salado area can be younger than the Cambro-Ordovician and, therefore, have only been affected by the Gondwanide metamorphism and deformation.

Implications for the late Palaeozoic evolution of northern Patagonia

From the regional point of view, the continental NW-SE trending Gondwanide orogenic belt of central-northern Patagonia can tectonically be divided from SW to NE into a forearc region, encompassing accretionary prisms exposed in southern Chile, the Tepuel Basin of central-southern Patagonia, and the basement complexes of the North Patagonian Andes. Then, the wide magmatic arc with migmatite massifs (covered mainly by the Cenozoic Somuncura plateau), and finally, the retroarc region separated from the foreland and the Río de la Plata Craton to the north by the Huincul Fault zone. Within this geodynamic scenario, the high-P/high-T thick-skinned fold-thrust belt of the MGMC lies in the retroarc region, towards the south of the Huincul Fault zone (Figure 1(a,b)).

Late Carboniferous-Permian crustal thickening related to the MGMC fold-and-thrust belt evolution is recorded by sheet-duplex stacking transported towards the S-SW over the magmatic arc. Thickening associated with high dT/dP metamorphism (Hyndman *et al.* 2005) and clockwise models in compressional retroarc regions characterize accretionary orogenic systems (e.g. Collins 2002; Collins and Richards 2008; Brown 2009, 2010). Contemporaneous crustal thickening also occurs in accretionary complexes and high-P basement complexes of the North Patagonian Andes exposed further SW in Chile and Bariloche (Willner *et al.* 2004; Oriolo *et al.* 2019), respectively, suggesting a coupled late Palaeozoic evolution (Figure 11). The widespread, coeval arc Gondwanide magmatism could also play a vital role in the crustal thickening by adding magma batches into the deep crust and as the heat source in the adjacent retroarc region (Oriolo *et al.* 2019). The arc magmatism becoming younger and hotter towards the retroarc combined with crustal thickening characterizes the 3D architecture in the inner hinge crust of an orocline (e.g. Ling *et al.* 2024), such occurs in the Arroyo Salado study area,

which is located along a curvature of the Gondwanide orocline to the SE (Figure 1(b)). Thus, the bending of the orogen can produced crustal thickening in retroarc and arc migration to inland (e.g. Ling *et al.* 2024).

In the Bariloche area, a comparable structural evolution of the F_2 folds development and associated S_2 foliation and L_2 lineation is constrained by monazite ages at 299 ± 8 and 302 ± 16 Ma during peak metamorphic conditions of $\sim 650^\circ\text{C}$ -11 kbar or shortly after achieved during prograde metamorphism and progressive deformation in a clockwise path (Oriolo *et al.* 2019). These ages are comparable to the oldest age in rocks of the Arroyo Salado study area, possibly related to the onset of development of the S_1 foliation and succeeded by the ubiquitous Permian formation of the younger S_2 (Figure 11(b)). Thus, the Gondwanide orogenic front migrated inboard across the continental margin from SW to NE, accompanied by the Gondwanide magmatism as revealed by the decrease in magmatic crystallization ages in the same direction, likely due to changing subduction dynamics related to slab shallowing (Figures 1(b) and 11(a)). Flat-slab subduction favours compression far from the trench and is associated with foreland arc migration/expansion and mountain-building/crustal thickening processes, resulting in advancing accretionary orogen (Martinod *et al.* 2020; Oriolo *et al.* 2023).

As occurred with magmatism, the ages of metamorphism and deformation also decrease towards the inland from the Upper Mississippian-Pennsylvanian accretionary prisms (Willner *et al.* 2004; Kato *et al.* 2008), Pennsylvanian-Cisuralian in the arc-related area (Renda *et al.* 2019; Oriolo *et al.* 2019, 2023; Marcos *et al.* 2020) including the retroarc Arroyo Salado area, to the Guadalupian-Lopingian in the foreland Cerro Los Viejos-Sierra de la Ventana (von Gosen *et al.* 1991), and reaching earliest Triassic ages in the Río de la Plata Craton (Zalba *et al.* 2007, Figure 11(a)). The age migration also agrees with a general trend of landward decrease of the metamorphic grade, in which the Patagonian subduction-related Panthalassan continental margin record the highest pressure rocks (blueschist facies, 350 – 500°C and 10–14 kbar) under progressive ductile conditions in the accretionary prisms of southern Chile (Willner *et al.* 2004; Kato *et al.* 2008, Figure 1(a,b)).

This pattern of coupled Late Carboniferous-Permian evolution to the north and south of the Huincul Fault zone may also account for the far-field stress and metamorphism in a rather intracontinental position, up to ~ 1300 km inboard of the inferred trench westward along the actual Chilean margin (e.g. Cawood *et al.* 2009). The kinematic activity with strain partitioning of the Huincul Fault zone as a first-order crustal discontinuity (e.g. Ramos *et al.* 2004; Gregori *et al.* 2008, 2013) could thus decouple

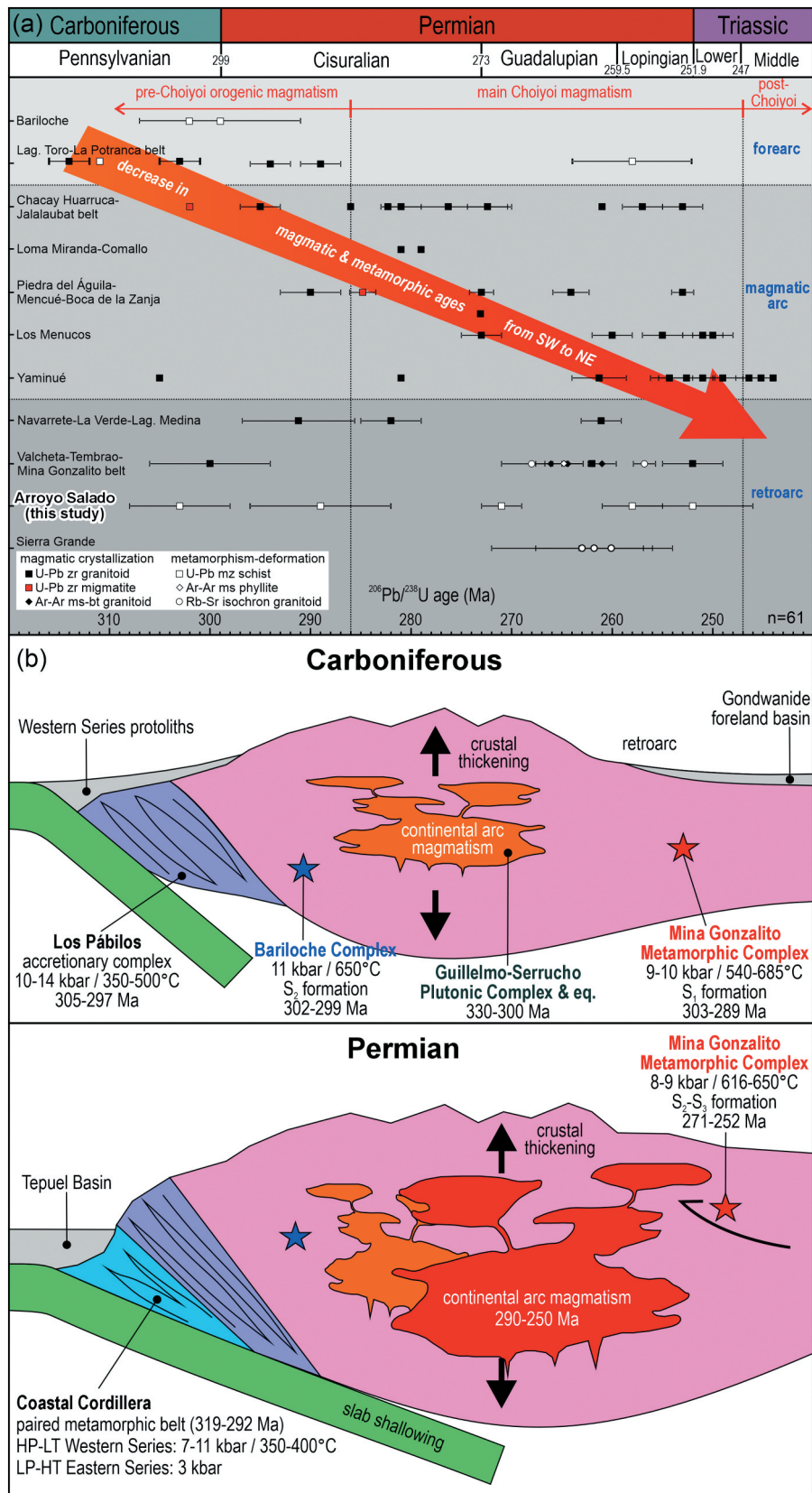


Figure 11. (a) Sketch with geographic distribution of the published radiometric data from northern region of Patagonia, prepared with data in Table S5-SOM and references therein. Key localities as in Figure 1b are located from forearc SW (Bariloche) to retroarc NE (Arroyo Salado) regions. Divisions of the Choiyoi Province magmatism after Sato *et al.* (2015). (b) Two stages in the geological evolution of the Gondwanide orogen built on the continental margin of Patagonia during the Carboniferous-Permian.

the eastern North Patagonian Massif retroarc region, containing the high-P sequence of the MGMC, towards the S-SW concerning the Cerro Los Viejos-Sierra de la Ventana foreland fold-thrust belt system to the N-NE, also with mylonite belts development and lower metamorphic grades (Trouw and de Wit 1999; Giacosa 2001; von Gosen 2003). Thus, the Patagonian segment of the Gondwanide orogen is doubly vergent to the north and south of the Huincul Fault zone.

Differences on both sides of the Huincul Fault zone have also been outlined for the Devonian (Marcos *et al.* 2023, and references therein). This distinct evolution of the late Palaeozoic tectonometamorphic evolution of Patagonia, recorded by mainly medium- to high-grade metamorphic rocks, contrasts significantly with the coeval upper crustal record of the Choiyoi Province (see above geological setting), indicating along-strike segmentation of the margin. The presence of large basement blocks with Laurentian affinity north of 36° S (e.g. San Rafael and Las Matras blocks, Figure 1(a)), which were juxtaposed by the Early to Middle Palaeozoic to the Gondwana margin (Ramos 2010, and references therein), may suggest that the proto-Andean region, including adjacent areas such as the Sierras Pampeanas, underwent cratonization before the Gondwanide Orogeny. In contrast, the Early to Middle Palaeozoic evolution of Patagonia was mainly characterized by alternating periods of retreating-advancing accretionary systems linked with subduction (Suárez *et al.* 2019; González and Giacosa 2021; Oriolo *et al.* 2023; Marcos *et al.* 2023). Though remnants of older Mesoproterozoic roots may be likely (e.g. Rapela *et al.* 2024), the pre-Gondwanide Patagonian record mainly comprises Early to Middle Palaeozoic metasedimentary rocks with subordinate meta-igneous intercalations. The lack of a thick lithospheric mantle by the early Carboniferous, which determines the presence of a stable continental crust, may thus explain the nearly ubiquitous Gondwanide metamorphic overprint of central-northern Patagonia basement complexes. The relative stabilization of this crustal segment was thus first achieved after widespread Gondwanide magmatism and crustal thickening (Oriolo *et al.* 2019, 2023).

It is strikingly to note along-strike segmentation of the continental Panthalassan margin of Gondwana, in which several Late Carboniferous to Permian metamorphic rocks documenting orogenic activity in western South America, the Antarctic Peninsula, Zealandia, and eastern Australian segments have also been recorded. The orogenic activity, together with the axis of the magmatic arc, parallels the plate margin and is also related to a pattern of inland decrease of the

metamorphic grade with strain localization and partitioning from the trench region to the rheologically weak retroarc lithosphere (Hyndman *et al.* 2005), possibly due to the heat provided by the migrating Gondwanide arc magmatism, and then the different segments of the Gondwanide fold-and-thrust belt system and the foreland basins (Samfrau Geosyncline of Du Toit 1927; Figure 1(a) and references therein). Hence, the continental geodynamic scenario for the Gondwanide orogen is an advancing-mode accretionary mountain chain collinear with the margin (Collins 2002; Cawood *et al.* 2009) instead of the result of a continental collision. The Gondwanide orogeny might thus be essentially linked to transpression due to advancing subduction along the Panthalassan margin of Gondwana.

Concluding remarks

The research reported in this contribution has characterized the P-T metamorphic conditions and the deformational structures of the Mina Gonzalito Metamorphic Complex in the Arroyo Salado area from northern Patagonia. Our new structural-microstructural, petrologic, and petrochronologic data constrain a thick-skinned fold-and-thrust belt spatially and temporally related to the geometry and kinematics of the El Jagüelito ductile shear zone. The deformation belt evolved in a general clockwise P-T-t-D path, where the rock trajectories across the various thrust sheets and duplexes have slightly diachronous P-T evolution. The deepest sheet close to the El Jagüelito shear zone reached maximum P-T conditions simultaneously at 9.9 kbar and 685°C, while the shallowest and furthest peak-P was 9.0–9.6 kbar at ~540°C and then the peak-T of 616–627°C at 8.0 kbar occurred. The right-lateral transpressive deformation of the shear zone and strain partitioning within the belt disturbed the regional isograds, upgrading them from 15–20°C/km during high-P metamorphism to 30°C/km at the Barrovian overprint. A single-phase progressive ductile deformation and regional medium- to high-pressure amphibolite facies metamorphic event characterize the resulting orogenic processes. Thorium-U-Pb monazite ages show the orogenesis span ~50 My (303–252 Ma), developed almost entirely within the Permian and ascribed to the Gondwanide orogeny. Our revised geotectonic scheme documents a coupled regional Late Palaeozoic tectonometamorphic and magmatic evolution to the building of the advancing-mode Gondwanide accretionary orogen along and across Patagonia South America, which can also be correlated with that occurs elsewhere on the Panthalassan margin of Gondwana.

Note

1. Whole-rock geochemical analyses of the samples are available upon request from the corresponding author.

Acknowledgments

We are deeply indebted to Ana María Sato and Ricardo Varela for all the help and support through the years they have given us, especially to P. D. González and M. Naipauer. We sincerely thank Lilian Carpintero, owner of the Santa Auriciana farm, for allowing us access to their farm and for their hospitality during our fieldwork. We also thank the three anonymous reviewers and the editor-in-chief of IJR for their valuable comments and contributions to improving the final version of the manuscript.

Disclosure statement

No potential conflict of interest was reported by the author(s).

Funding

This work was supported by the SEGEMAR; Universidad Nacional de Río Negro under Grant PI-UNRN-2021-40-A-959; Ministerio de Ciencia, Tecnología e Innovación Productiva, Agencia Nacional de Promoción Científica y Tecnológica under Grant FONCYT-PICT-2021-01081, and CONICET under Grant PIP-112202001000990.

ORCID

Pablo D. González  <http://orcid.org/0000-0003-3498-8128>

References

- Ballivián Justiniano, C., Oriolo, S., Basei, M., Lanfranchini, M., Christiansen, R., Uriz, N., Vázquez Lucero, S., Del Bono, D., Forster, M., Etcheverry, R., Tassinari, C., Comerio, M., and Prezzi, C., 2023, The Gondwanide deformation along the southwestern border of the Río de la Plata Craton: Geochemical and geochronological constraints on ductile shear zones from the Ventania System basement: Argentina: *Journal of South American Earth Sciences*, v. 124, p. 104275. doi:10.1016/j.jsames.2023.104275
- Basei, M., Varela, R., Passarelli, C., Siga, O., Jr., Cingolani, C., Sato, A., and González, P., 2005, The crystalline basement in the north of Patagonia: Isotopic ages and regional characteristics: *Gondwana 12: Geological and Biological Heritage of Gondwana*, Abstracts, v. CD, p. 62.
- Basei, M., Varela, R., Sato, A., Siga, O., Jr., and Llambias, E., 2002, Geocronología sobre rocas del Complejo Yaminué, Macizo Norpatagónico, Río Negro, Argentina, in *Proceedings, 15th Congreso Geológico Argentino*, El Calafate, Santa Cruz, v. 3, p. 117–122.
- Berman, R., 1991, Thermobarometry using multi-equilibrium calculations: A new technique, with petrological applications: *Canadian Mineralogist*, v. 29, p. 833–855.
- Berman, R., 2007, winTWQ (version 2.3): A software package for performing internally-consistent thermobarometric calculations: Geological Survey of Canada: Open File, v. 5462, ed. 2.32. p. 41.
- Berman, R., and Aranovich, L., 1996, Optimized standard state and solution properties of minerals: Contributions to Mineralogy and Petrology, v. 126, no. 1–2, p. 1–24. doi: 10.1007/s004100050232
- Blewett, S., and Phillips, D., 2016, An overview of Cape Fold Belt geochronology: implications for sediment provenance and the timing of orogenesis, in Linol, B., and de Wit, M., eds. *Origin and evolution of the Cape Mountains and Karoo Basin: Regional geology reviews*: Cham, Springer, pp. 45–55. doi:10.1007/978-3-319-40859-0_5
- Blewett, S., Phillips, D., and Matchan, E., 2019, Provenance of Cape Supergroup sediments and timing of Cape Fold Belt orogenesis: Constraints from high-precision $^{40}\text{Ar}/^{39}\text{Ar}$ dating of muscovite: *Gondwana Research*, v. 70, p. 201–221. doi:10.1016/j.gr.2019.01.009
- Bosse, V., and Villa, I., 2019, Petrochronology and hydrochronology of tectono-metamorphic events: *Gondwana Research*, v. 71, p. 76–90. doi:10.1016/j.gr.2018.12.014
- Brown, M., 2009, Metamorphic patterns in orogenic systems and the geological record, in Cawood, P., and Kröner, A. eds. *Accretionary orogens in space and time*: Geological society, London, Special Publications, Vol. 318, pp. 37–74.
- Brown, M., 2010, Paired metamorphic belts revisited: *Gondwana Research*, v. 18, no. 1, p. 46–59. doi: 10.1016/j.gr.2009.11.004
- Castle, J., and Craddock, C., 1975, Deposition and metamorphism of the Polarstar Formation (Permian), Ellsworth mountains: *Antarctic Journal*, v. 10, p. 239–241.
- Cawood, P., 2005, Terra Australis Orogen: Rodinia breakup and development of the Pacific and Iapetus margins of Gondwana during the Neoproterozoic and Paleozoic: *Earth-Science Reviews*, v. 69, no. 3–4, p. 249–279. doi: 10.1016/j.earscirev.2004.09.001
- Cawood, P., Kröner, A., Collins, W., and Kusky, T., 2009, Accretionary orogens through Earth history, in Cawood, P., and Kröner, A. eds. *Earth accretionary systems in space and time*: The Geological Society, London, Special Publications, Vol. 318, pp. 1–36.
- Chatterjee, N., and Froese, E., 1975, A thermodynamic study of the pseudobinary join muscovite-paragonite in the system $\text{KAlSi}_3\text{O}_8\text{-NaAlSi}_3\text{O}_8\text{-Al}_2\text{O}_3\text{-SiO}_2\text{-H}_2\text{O}$: *American Mineralogist*, v. 60, p. 985–993.
- Chernicoff, C., and Caminos, R., 1996, Estructura y metamorfismo del Complejo Yaminué, Macizo Nordpatagónico oriental, provincia de Río Negro: *Revista de la Asociación Geológica Argentina*, v. 51, p. 107–118.
- Christiansen, R., Ballivián Justiniano, C., Oriolo, S., Gianni, G., García, H.P.A., Martínez, M.P., Kostadinoff, J., et al. 2021, Crustal architecture and tectonic evolution of the southernmost Río de la Plata Craton and its Neoproterozoic–Paleozoic sedimentary cover: Insights from 3D litho-constrained stochastic inversion models: *Precambrian Research*, v. 362, p. 106307. doi:10.1016/j.precamres.2021.106307
- Cobbold, P., Gapais, D., and Rosello, E., 1991, Partitioning of transpressive motions within a sigmoidal fold belt: The Variscan Sierras Australes, Argentina: *Journal of Structural Geology*, v. 13, no. 7, p. 743–758. doi: 10.1016/0191-8141(91)90001-Y

- Collins, W., 2002, Nature of extensional accretionary orogens: *Tectonics*, v. 21, no. 4, p. 1024. doi: [10.1029/2000TC001272](https://doi.org/10.1029/2000TC001272)
- Collins, W., and Richards, S., 2008, Geodynamic significance of S-type granites in circum-Pacific orogens: *Geology*, v. 36, no. 7, p. 559–562. doi: [10.1130/G24658A.1](https://doi.org/10.1130/G24658A.1)
- Dalziel, I., and Grunow, A., 1992, Late Gondwanide tectonic rotations within Gondwanaland: *Tectonics*, v. 11, no. 3, p. 603–606. doi: [10.1029/91TC02365](https://doi.org/10.1029/91TC02365)
- Dubosq, R., Camacho, A., Rogowitz, A., Zhang, S., and Gault, B., 2024, Influence of high-strain deformation on major element mobility in garnet: Nanoscale evidence from atom probe tomography: *Journal of Metamorphic Geology*, v. 42, no. 3, p. 355–372. doi: [10.1111/jmg.12758](https://doi.org/10.1111/jmg.12758)
- Du Toit, A., 1927, A geological comparison of South America with South Africa, Washington, Carnegie Institution.
- Du Toit, A., 1937, Our wandering continents; an hypothesis of continental drifting, London, Oliver and Boyd, p. 394.
- Engi, M., 2017, Petrochronology based on REE-minerals: monazite, allanite, xenotime, apatite: *Reviews in Mineralogy and Geochemistry*, v. 83, no. 1, p. 365–418. doi: [10.2138/rmg.2017.83.12](https://doi.org/10.2138/rmg.2017.83.12)
- Falco, J., Hauser, N., Scivetti, N., Reimold, W., and Folguera, A., 2022, The origin of Patagonia: Insights from Permian to Middle Triassic magmatism of the North Patagonian Massif: *Geological Magazine*, v. 159, no. 9, p. 1490–1512. doi: [10.1017/S0016756822000450](https://doi.org/10.1017/S0016756822000450)
- Fossen, H., Cavalcante, G., Pinheiro, R., and Archanjo, C., 2018, Deformation-progressive or multiphase?: *Journal of Structural Geology*, v. 125, p. 82–99. doi: [10.1016/j.jsg.2018.05.006](https://doi.org/10.1016/j.jsg.2018.05.006)
- Fossen, H., Teyssier, C., and Whitney, D., 2013, Transtensional folding: *Journal of Structural Geology*, v. 56, p. 89–102. doi: [10.1016/j.jsg.2013.09.004](https://doi.org/10.1016/j.jsg.2013.09.004)
- Fuhrman, M., and Lindsley, D., 1988, Ternary feldspar modeling and thermometry: *American Mineralogist*, v. 73, p. 201–215.
- Gaidies, F., 2021, Disequilibrium microstructures of metamorphic rocks, in Alderton, D., and Elias, S., eds. *Encyclopedia of geology*: Amsterdam, Elsevier, Vol. 2, pp. 389–396. doi: [10.1016/B978-0-08-102908-4.00001-1](https://doi.org/10.1016/B978-0-08-102908-4.00001-1)
- García, V., González, S., Tassinari, C., and Sato, K., 2014, U-Pb and Nd data from Peñas Blancas Pluton, Northpatagonian Massif, Argentina: 9th South American Symposium on Isotope Geology Program and Abstracts, Sao Paulo, Brazil, p. 190.
- Giacosa, R., 1994, Evolución tectónica pre-Cretácica del margen Atlántico del Macizo Nordpatagónico, Argentina: *Zentralblatt für Geologie und Paläontologie*, v. v. I, p. 687–700.
- Giacosa, R., 2001, Zonas de cizalla frágil-dúctil neopaleozoicas en el nordeste de la Patagonia: *Revista de la Asociación Geológica Argentina*, v. 56, p. 131–140.
- González, P., and Giacosa, R., 2021, Rocas metamórficas e ígneas del Paleozoico, in Giacosa, R., ed. *Relatorio de la Geología y Recursos Naturales de la Provincia de Chubut*: Buenos Aires, SEGEMAR, pp. 47–104.
- González, P., Naipauer, M., Sato, A., Varela, R., Basei, M., Cávana, M., Vlach, S., Arce, M., and Parada, M., 2021, Early Paleozoic structural and metamorphic evolution of the Transpatagonian Orogen related to Gondwana assembly: *International Journal of Earth Sciences*, v. 110, no. 1, p. 81–111. doi: [10.1007/s00531-020-01939-0](https://doi.org/10.1007/s00531-020-01939-0)
- González, P., Sato, A., Llambias, E., and Varela, R., 2008b, Geología del Corrimiento Piedras Coloradas, basamento ígneo-metamórfico de Las Grutas, Río Negro. *Proceedings 17th Congreso Geológico Argentino*, San Salvador de Jujuy, Jujuy, v. 2, p. 845–846.
- González, P., Sato, A., Naipauer, M., Varela, R., Basei, M., Sato, K., Llambias, E.J., Chemale, F., and Dorado, A.C., 2018, Patagonia-Antarctica Early Paleozoic conjugate margins: Cambrian synsedimentary silicic magmatism, U-Pb dating of K-bentonites, and related volcanogenic rocks: *Gondwana Research*, v. 63, p. 186–225. doi: [10.1016/j.gr.2018.05.015](https://doi.org/10.1016/j.gr.2018.05.015)
- González, P., Varela, R., Sato, A., Llambias, E., and González, S., 2008a, Dos fajas estructurales distintas en el Complejo Mina Gonzalito, Río Negro. *Proceedings 17th Congreso Geológico Argentino*, San Salvador de Jujuy, Jujuy, v. 2, p. 847–848.
- Greco, G., González, S., Sato, A., and González, P., 2014, Nueva datación en circones detríticos para el Complejo Mina Gonzalito, Provincia de Río Negro. *Proceedings 19th Congreso Geológico Argentino*, Córdoba, v. CD, p. 1454–1455.
- Greco, G., González, S., Sato, A., González, P., Basei, M., Llambias, E., and Varela, R., 2017, The Nahuel Niyeu basin: A Cambrian forearc basin in the eastern North Patagonian Massif: *Journal of South American Earth Sciences*, v. 79, p. 111–136. doi: [10.1016/j.jsames.2017.07.009](https://doi.org/10.1016/j.jsames.2017.07.009)
- Gregori, D., Kostadinoff, J., Alvarez, G., Raniolo, A., Strazzere, L., Martínez, J.C., and Barros, M., et al. 2013, Preandean geological configuration of the eastern North Patagonian Massif, Argentina: *Geoscience Frontiers*, v. 4, no. 6, p. 693–708. doi: [10.1016/j.gsf.2013.01.001](https://doi.org/10.1016/j.gsf.2013.01.001)
- Gregori, D., Kostadinoff, J., Strazzere, L., and Raniolo, A., 2008, Tectonic significance and consequences of the Gondwanide orogeny in northern Patagonia, Argentina: *Gondwana Research*, v. 14, no. 3, p. 429–450. doi: [10.1016/j.gr.2008.04.005](https://doi.org/10.1016/j.gr.2008.04.005)
- Gregori, D., Strazzere, L., Barros, M., Benedini, L., Marcos, P., and Kostadinoff, J., et al. 2021, The Mengué Batholith: Permian episodic arc-related magmatism in the western North Patagonian Massif, Argentina: *International Geology Review*, v. 63, no. 3, p. 317–341. doi: [10.1080/00206814.2019.1710865](https://doi.org/10.1080/00206814.2019.1710865)
- Hervé, F., Calderón, M., Fanning, M., Kraus, S., and Pankhurst, R., 2010, Geocronología SHRIMP del basamento de la Cuenca de Magallanes, Tierra del Fuego: plutonismo Cámbrico y metamorfismo Permiano de alto grado: *Andean Geology*, v. 37, no. 2, p. 253–275. doi: [10.5027/andgeoV37n2-a01](https://doi.org/10.5027/andgeoV37n2-a01)
- Hervé, F., Calderón, M., Fanning, M., Kraus, S., Pankhurst, R., Quezada, P., et al. 2018, The country rocks of Devonian magmatism in the North Patagonian Massif and Chaitenia: *Andean Geology*, v. 45, no. 3, p. 301–317. doi: [10.5027/andgeoV45n3-3117](https://doi.org/10.5027/andgeoV45n3-3117)
- Holdaway, M., 2000, Application of new experimental and garnet Margules data to the garnet-biotite geothermometer: *American Mineralogist*, v. 85, no. 7–8, p. 881–892. doi: [10.2138/am-2000-0701](https://doi.org/10.2138/am-2000-0701)
- Hyndman, R., Currie, C., and Mazzotti, S., 2005, Subduction zone backarcs, mobile belts, and orogenic heat: *GSA Today: A Publication of the Geological Society of America*, v. 15, no. 2, p. 4–10. doi: [10.1130/1052-5173\(2005\)015<4:SZBMB>2.0.CO;2](https://doi.org/10.1130/1052-5173(2005)015<4:SZBMB>2.0.CO;2)
- Jessop, K., Daczko, N., and Piazzolo, S., 2020, Metamorphism in the New England Orogen, eastern Australia: A review:

- Australian Journal of Earth Sciences, v. 67, no. 4, p. 453–478. doi: [10.1080/08120099.2020.1685000](https://doi.org/10.1080/08120099.2020.1685000)
- Johnson, S., 1999, Porphyroblast microstructures: A review of current and future trends: *American Mineralogist*, v. 84, no. 11–12, p. 1711–1726. doi: [10.2138/am-1999-11-1202](https://doi.org/10.2138/am-1999-11-1202)
- Jones, R., Holdsworth, R., Clegg, P., McCaffrey, E., and Tavarnerelli, K., 2004, Inclined transpression: *Journal of Structural Geology*, v. 26, no. 8, p. 1531–1548. doi: [10.1016/j.jsg.2004.01.004](https://doi.org/10.1016/j.jsg.2004.01.004)
- Kato, T., Sharp, W., and Godoy, E., 2008, Inception of a Devonian subduction zone along the southwestern Gondwana margin: 40 Ar–39 Ar dating of eclogite–amphibolite assemblages in blueschist boulders from the Coastal Range of Chile (41°S): *Canadian Journal of Earth Sciences*, v. 45, no. 3, p. 337–351. doi: [10.1139/E08-006](https://doi.org/10.1139/E08-006)
- Kay, S., Ramos, V., Mpodozis, C., and Sruoga, P., 1989, Late Paleozoic to Jurassic silicic magmatism at the Gondwana margin: Analogy to the Middle Proterozoic in North America?: *Geology*, v. 17, no. 4, p. 324–328. doi: [10.1130/0091-7613\(1989\)017<0324:LPTJSM>2.3.CO;2](https://doi.org/10.1130/0091-7613(1989)017<0324:LPTJSM>2.3.CO;2)
- Kleiman, L., and Japas, M., 2009, The Choiyoi volcanic province at 34°S–36°S (San Rafael, Mendoza, Argentina): Implications for the Late Palaeozoic evolution of the southwestern margin of Gondwana: *Tectonophysics*, v. 473, no. 3–4, p. 283–299. doi: [10.1016/j.tecto.2009.02.046](https://doi.org/10.1016/j.tecto.2009.02.046)
- Lardeaux, J.-M., 2024, Metamorphism and linked deformation in understanding tectonic processes at varied scales: *Comptes Rendus Géoscience*, v. 356, no. S2, p. 1–25. doi: [10.5802/crgeos.204](https://doi.org/10.5802/crgeos.204)
- Lawver, L., Gahagan, L., and Dalziel, I., 1998, A tight fit–Early Mesozoic Gondwana, a plate reconstruction perspective: *Memoir National Institute of Polar Research, Special Issue* v. 53, p. 214–229.
- Likhanov, I., 2020, Metamorphic indicators for collision, extension, and shear zone geodynamic settings of the Earth's crust: *Petrology*, v. 28, no. 1, p. 1–16. doi: [10.1134/S086959112001004X](https://doi.org/10.1134/S086959112001004X)
- Ling, J., Li, P., Yuan, C., Rosenbaum, G., Sun, M., Li, Z., and Narantsetseg, T., et al. 2024, The bending of a supra-subduction zone produced crustal thickening and arc migration of the Mongolian Orocline: *Communications Earth & Environment*, v. 5, no. 1, p. article 329. doi: [10.1038/s43247-024-01492-7](https://doi.org/10.1038/s43247-024-01492-7)
- Llambias, E., Quenardelle, S., and Montenegro, T., 2003, The Choiyoi group from central Argentina: A subalkaline transitional to alkaline association in the craton adjacent to the active margin of the Gondwana continent: *Journal of South American Earth Sciences*, v. 16, no. 4, p. 243–257. doi: [10.1016/S0895-9811\(03\)00070-1](https://doi.org/10.1016/S0895-9811(03)00070-1)
- Llambias, E., Varela, R., Basei, M., and Sato, A., 2002, Deformación dúctil y metamorfismo neopaleozoico en el área de Yaminué y su relación con la Fase Orogénica San Rafael. *Proceedings 15 th Congreso Geológico Argentino, El Calafate, Santa Cruz*, v. 3, p. 117–122.
- López-Gamundí, O., and Rossello, E., 1998, Basin fill evolution and palaeotectonic patterns along the Samfrau geosyncline: The Sauce Grande basin–Ventana fold belt (Argentina) and Karoo basin–Cape fold belt (South Africa): *Geologische Rundschau*, v. 86, no. 4, p. 819–834. doi: [10.1007/s005310050179](https://doi.org/10.1007/s005310050179)
- Lü, Z., Yan, J., and Li, J., 2023, The fate of kyanite in ultrahigh-pressure metasedimentary rocks, southwestern Tianshan, NW China: *Lithos*, v. 458–459, p. 107356. doi: [10.1016/j.lithos.2023.107356](https://doi.org/10.1016/j.lithos.2023.107356)
- Lucassen, F., Franz, G., and Laber, A., 1999, Permian high pressure rocks—the basement of the Sierra de Limón Verde in Northern Chile: *Journal of South American Earth Sciences*, v. 12, no. 2, p. 183–199. doi: [10.1016/S0895-9811\(99\)00013-9](https://doi.org/10.1016/S0895-9811(99)00013-9)
- Ludwig, K., 2001, User manual for Isoplot/Ex (rev. 2.49): A geochronological toolkit for Microsoft Excel: Berkeley Geochronology Center Special Publication, v. 1a, p. 55.
- Marcos, P., Gregori, D., Benedini, L., Barros, M., Strazzere, L., and Pivetta, C.P., et al. 2018, Pennsylvanian glacial marine sedimentation in the Cushamen Formation, western North Patagonian Massif: *Geoscience Frontiers*, v. 9, no. 2, p. 485–504. doi: [10.1016/j.gsf.2017.05.005](https://doi.org/10.1016/j.gsf.2017.05.005)
- Marcos, P., Pavón Pivetta, C., Benedini, L., Gregori, D., et al. 2020, Late Paleozoic geodynamic evolution of the western North Patagonian Massif and its tectonic context along the southwestern Gondwana margin: *Lithos*, v. 376–377, p. 105801. doi: [10.1016/j.lithos.2020.105801](https://doi.org/10.1016/j.lithos.2020.105801)
- Marcos, P., Renda, E., González, P., Oriolo, S., Scivetti, N., Benedini, L., Gerales, M., Gregori, D., Yoya, M.B., Bahía, M., et al. 2023, Devonian to early carboniferous retreating—advancing subduction switch in the Northwestern Patagonia Accretionary Orogen: U–Pb and Lu–Hf Isotopic Insights: *Tectonics*, v. 42, no. 11, p. e2022TC007533. doi: [10.1029/2022TC007533](https://doi.org/10.1029/2022TC007533)
- Martin, M., Kato, T., Rodríguez, C., Godoy, E., Duhart, P., McDonough, M., and Campos, A., 1999, Evolution of the late Paleozoic accretionary complex and overlying forearc-magmatic arc, south central Chile (38°–41°S): Constraints for the tectonic setting along the southwestern margin of Gondwana: *Tectonics*, v. 18, no. 4, p. 582–605. doi: [10.1029/1999TC900021](https://doi.org/10.1029/1999TC900021)
- Martinod, J., Gérault, M., Husson, L., and Regard, V., 2020, Widening of the Andes: An interplay between subduction dynamics and crustal wedge tectonics: *Earth-Science Reviews*, v. 204, p. 103170. doi: [10.1016/j.earscirev.2020.103170](https://doi.org/10.1016/j.earscirev.2020.103170)
- Montel, J., Foret, S., Veschambre, M., Nicollet, C., and Provost, A., 1996, Electron microprobe dating of monazite: *Chemical Geology*, v. 131, no. 1–4, p. 37–53. doi: [10.1016/0009-2541\(96\)00024-1](https://doi.org/10.1016/0009-2541(96)00024-1)
- Oriolo, S., González, P., Renda, E., Basei, M., Otamendi, J., Cordenons, P., Marcos, P., Yoya, M.B., Ballivián Justiniano, C. A., and Suárez, R., et al. 2023, Linking accretionary orogens with continental crustal growth and stabilization: Lessons from Patagonia: *Gondwana Research*, v. 121, p. 368–382. doi: [10.1016/j.gr.2023.05.011](https://doi.org/10.1016/j.gr.2023.05.011)
- Oriolo, S., Schulz, B., González, P.D., Bechis, F., Olaizola, E., Krause, J., Renda, E.M., and Vizán, H., et al. 2019, The Late Paleozoic tectonometamorphic evolution of Patagonia revisited: Insights from the pressure–temperature–deformation–time (P–T–D–t) path of the Gondwanide basement of the North Patagonian Cordillera (Argentina): *Tectonics*, v. 38, no. 7, p. 2378–2400. doi: [10.1029/2018TC005358](https://doi.org/10.1029/2018TC005358)
- Oriolo, S., Schulz, B., Hueck, M., Oyhantçabal, P., Heidelbach, F., Sosa, G., van den Kerkhof, A., Wemmer, K., Fossen, H., Druguet, E., Walter, J., Cavalcante, C., Siegesmund, S., et al. 2022, The petrologic and petrochronologic record of progressive vs. polyphase deformation: Opening the analytical

- toolbox: *Earth-Science Reviews*, v. 234, p. 104235. doi:[10.1016/j.earscirev.2022.104235](https://doi.org/10.1016/j.earscirev.2022.104235)
- Pankhurs, R., Rapela, C., Lopez de Luchi, M., 2014, The Gondwana connections of northern Patagonia: *Journal of the Geological Society*, v. 171, no. 3, p. 313–328. doi:[10.1144/jgs2013-081](https://doi.org/10.1144/jgs2013-081)
- Pankhurst, R., Rapela, C., Fanning, C., and Márquez, M., et al. 2006, Gondwanide continental collision and the origin of Patagonia: *Earth-Science Reviews*, v. 76, no. 3–4, p. 235–257. doi:[10.1016/j.earscirev.2006.02.001](https://doi.org/10.1016/j.earscirev.2006.02.001)
- Peillod, A., Patten, C., Drüppel, C., Beranoaguirre, K., Zeh, A., Gudelius, D., Hector, S., Majka, J., Kleine-Marshall, B.I., Karlson, A., Gerdes, A., Kolb, J., et al. 2024, Disruption of a high-pressure unit during exhumation: Example of the Cycladic Blueschist unit (Thera, los and Naxos islands, Greece): *Journal of Metamorphic Geology*, v. 42, no. 2, p. 225–255. doi:[10.1111/jmg.12753](https://doi.org/10.1111/jmg.12753)
- Ramos, V., 1984, Patagonia: ¿un continente Paleozoico a la deriva? *Proceedings 9 th Congreso Geológico Argentino*, San Carlos de Bariloche, Río Negro, v. 2, p. 311–325.
- Ramos, V., 2008, Patagonia: A Paleozoic continent adrift?: *Journal of South American Earth Sciences*, v. 26, no. 3, p. 235–251. doi: [10.1016/j.jsames.2008.06.002](https://doi.org/10.1016/j.jsames.2008.06.002)
- Ramos, V., 2010, The Grenville-age basement of the Andes: *Journal of South American Earth Sciences*, v. 29, no. 1, p. 77–91. doi: [10.1016/j.jsames.2009.09.004](https://doi.org/10.1016/j.jsames.2009.09.004)
- Ramos, V., Riccardi, A., and Roller, E., 2004, Límites naturales del norte de la Patagonia: *Revista de la Asociación Geológica Argentina*, v. 59, p. 785–786.
- Rapalini, A., 1998, Syntectonic magnetization of the mid-Paleozoic Sierra Grande Formation: Further constraints on the tectonic evolution of Patagonia: *Journal of the Geological Society*, v. 155, no. 1, p. 105–114. doi: [10.1144/gsjgs.155.1.0105](https://doi.org/10.1144/gsjgs.155.1.0105)
- Rapela, C., García, M., Hervé, F., Pankhurst, R., Calderón, M., Fanning, C.M., and Verdecchia, S.O., et al. 2024, Late Paleozoic magmatism and foreland deformation associated with opening and closing of marginal basins in the North Patagonian Andes: *Journal of the Geological Society*, v. 181, no. 2, p. jgs2023–171. doi:[10.1144/jgs2023-171](https://doi.org/10.1144/jgs2023-171)
- Renda, E., Alvarez, D., Prezzi, C., Oriolo, S., and Vizán, H., et al. 2019, Inherited basement structures and their influence in foreland evolution: A case study in Central Patagonia, Argentina: *Tectonophysics*, v. 772, p. 228232. doi:[10.1016/j.tecto.2019.228232](https://doi.org/10.1016/j.tecto.2019.228232)
- Renda, E., González, P., Vizán, H., Oriolo, S., Prezzi, C., Ruiz González, V., Schulz, B., Krause, J., and Basei, M., et al. 2021, Igneous-metamorphic basement of Taquetrén Range, Patagonia, Argentina: A key locality for the reconstruction of the Paleozoic evolution of Patagonia: *Journal of South American Earth Sciences*, v. 106, p. 103045. doi:[10.1016/j.jsames.2020.103045](https://doi.org/10.1016/j.jsames.2020.103045)
- Rocha-Campos, A., Basei, M., Nutman, A., Kleiman, L., Varela, R., Llambias, E., Canile, F.M., da Rosa, O.D.C.R., et al. 2011, 30 million years of Permian volcanism recorded in the Choiyoi igneous province (W Argentina) and their source for younger ash fall deposits in the Paraná Basin: SHRIMP U–Pb zircon geochronology evidence: *Gondwana Research*, v. 19, no. 2, p. 509–523. doi:[10.1016/j.gr.2010.07.003](https://doi.org/10.1016/j.gr.2010.07.003)
- Sato, A., Llambias, E., Basei, M., and Castro, C., 2015, Three stages in the Late Paleozoic to Triassic magmatism of south-western Gondwana, and the relationships with the volcanogenic events in coeval basins: *Journal of South American Earth Sciences*, v. 63, p. 48–69. doi:[10.1016/j.jsames.2015.07.005](https://doi.org/10.1016/j.jsames.2015.07.005)
- Schulz, B., 2021, Monazite microstructures and their interpretation in petrochronology: *Frontiers in Earth Sciences*, v. 9, p. 668566. doi:[10.3389/feart.2021.668566](https://doi.org/10.3389/feart.2021.668566)
- Shaanan, U., Rosenbaum, G., Li, P., and Vasconcelos, P., 2014, Structural evolution of the early Permian Nambucca Block (New England Orogen, eastern Australia) and implications for oroclinal bending: *Tectonics*, v. 33, no. 7, p. 1425–1443. doi: [10.1002/2013TC003426](https://doi.org/10.1002/2013TC003426)
- Sonder, L., and Chamberlain, P., 1992, Tectonic controls of metamorphic field gradients: *Earth and Planetary Science Letters*, v. 111, no. 2–4, p. 517–535. doi: [10.1016/0012-821X\(92\)90200-F](https://doi.org/10.1016/0012-821X(92)90200-F)
- Spear, F., 2010, Monazite–allanite phase relations in metapelites: *Chemical Geology*, v. 279, no. 1–2, p. 55–62. doi: [10.1016/j.chemgeo.2010.10.004](https://doi.org/10.1016/j.chemgeo.2010.10.004)
- Suárez, R., González, P., and Ghiglione, M., 2019, A review on the tectonic evolution of the Paleozoic–Triassic basins from Patagonia: Record of protracted westward migration of the pre-Jurassic subduction zone: *Journal of South American Earth Sciences*, v. 95, p. 102256. doi:[10.1016/j.jsames.2019.102256](https://doi.org/10.1016/j.jsames.2019.102256)
- Suzuki, K., Adachi, M., and Kajizuka, I., 1994, Electron microprobe observations of Pb diffusion in metamorphosed detrital monazites: *Earth and Planetary Science Letters*, v. 128, no. 3–4, p. 391–405. doi: [10.1016/0012-821X\(94\)90158-9](https://doi.org/10.1016/0012-821X(94)90158-9)
- Tenczer, V., and Stüwe, K., 2003, The metamorphic field gradient in the eclogite type locality, Koralpe region, Eastern Alps: *Journal of Metamorphic Geology*, v. 21, no. 4, p. 377–393. doi: [10.1046/j.1525-1314.2003.00448.x](https://doi.org/10.1046/j.1525-1314.2003.00448.x)
- ten Grotenhuis, S., Trouw, R., and Passchier, C., 2003, Evolution of mica fish in mylonitic rocks: *Tectonophysics*, v. 372, no. 1–2, p. 1–21. doi: [10.1016/S0040-1951\(03\)00231-2](https://doi.org/10.1016/S0040-1951(03)00231-2)
- Tickyj, H., Dimieri, L., Llambias, E., and Sato, A., 1997, Cerro de los Viejos (38°28'S–64°26'O): cizallamiento dúctil en el sudeste de La Pampa: *Revista de la Asociación Geológica Argentina*, v. 52, p. 311–321.
- Trouw, R., and de Wit, M., 1999, Relation between the Gondwanide Orogen and contemporaneous intracratonic deformation: *Journal of African Earth Sciences*, v. 28, no. 1, p. 203–213. doi: [10.1016/S0899-5362\(99\)00024-X](https://doi.org/10.1016/S0899-5362(99)00024-X)
- Varela, R., Basei, M., Cingolani, C., Siga, O., and Passarelli, C.R., et al. 2005, El basamento cristalino de los Andes Norpatagónicos en Argentina: geocronología e interpretación tectónica: *Andean Geology*, v. 32, no. 2, p. 167–187. doi:[10.4067/S0716-02082005000200001](https://doi.org/10.4067/S0716-02082005000200001)
- Varela, R., Dalla Salda, L., and Cingolani, C., 1985, Estructura y composición geológica de las Sierras Colorado, Chasicó y Cortapié, Sierras Australes de Buenos Aires: *Revista de la Asociación Geológica Argentina*, v. 40, p. 254–261.
- Varela, R., González, P., Basei, M., and Sato, K., 2011, Edad del Complejo Mina Gonzalito: revisión y nuevos datos. *Proceedings 18 th Congreso Geológico Argentino*, Neuquén, v. CD, p. 127–128.
- Varela, R., González, P., Philipp, R., and Sato, A., et al., 2014, Isótopos de estroncio en calcáreos del noreste patagónico: resultados preliminares: *Revista de la Asociación Geológica Argentina*, v. 71, p. 526–536.
- Vermeesch, P., 2012, On the visualisation of detrital age distributions: *Chemical Geology*, v. 312–313, p. 190–194. doi:[10.1016/j.chemgeo.2012.04.021](https://doi.org/10.1016/j.chemgeo.2012.04.021)

- von Gosen, W., 2002, Polyphase structural evolution in the northeastern segment of the North Patagonian Massif (southern Argentina): *Journal of South American Earth Sciences*, v. 15, p. 591–623. doi:[10.1016/S0895-9811\(02\)00111-6](https://doi.org/10.1016/S0895-9811(02)00111-6)
- von Gosen, W., 2003, Thrust tectonics in the North Patagonian Massif (Argentina): Implications for a Patagonian plate: *Tectonics*, v. 22, no. 1, p. 1005. doi: [10.1029/2001TC901039](https://doi.org/10.1029/2001TC901039)
- von Gosen, W., 2009, Stages of Late Palaeozoic deformation and intrusive activity in the western part of the North Patagonian Massif (southern Argentina) and their geotectonic implications: *Geological Magazine*, v. 146, no. 1, p. 48–71. doi: [10.1017/S0016756808005311](https://doi.org/10.1017/S0016756808005311)
- von Gosen, W., Buggisch, W., and Krumm, S., 1991, Metamorphic and deformation mechanisms in the Sierras Australes fold thrust belt (Buenos Aires, Province, Argentina): *Tectonophysics*, v. 185, no. 3–4, p. 335–356. doi: [10.1016/0040-1951\(91\)90453-Y](https://doi.org/10.1016/0040-1951(91)90453-Y)
- Wendt, A., Vaughan, A., and Tate, A., 2008, Metamorphic rocks in the Antarctic Peninsula region: *Geological Magazine*, v. 145, no. 5, p. 655–676. doi: [10.1017/S0016756808005050](https://doi.org/10.1017/S0016756808005050)
- Whitney, D., Paterson, S., Schmidt, K., and Glazner, A., et al., 2004, Growth and demise of continental arcs and orogenic plateaux in the North American Cordillera: From Baja to British Columbia, in Grocott, J., McCaffrey, K., Taylor, G., and Tikoff, B. eds. *Vertical coupling and decoupling in the lithosphere*: Geological Society, London, Special Publication, Vol. 227, pp. 167–175.
- Willner, A., Glodny, J., Gerya, T., Godoy, E., et al. 2004, A counterclockwise P-T-t path of high-pressure/low-temperature rocks from the Coastal Cordillera accretionary complex of south-central Chile: Constraints for the earliest stage of subduction mass flow: *Lithos*, v. 75, no. 3–4, p. 283–310. doi:[10.1016/j.lithos.2004.03.002](https://doi.org/10.1016/j.lithos.2004.03.002)
- Willner, A., Sepúlveda, F., Hervé, F., Massonne, H., Sudo, M., et al. 2009, Conditions and timing of pumpellyite–actinolite-facies metamorphism in the Early Mesozoic Frontal Accretionary Prism of the Madre de Dios Archipelago (Latitude 50°20'S; Southern Chile): *Journal of Petrology*, v. 50, no. 11, p. 2127–2155. doi:[10.1093/petrology/egp071](https://doi.org/10.1093/petrology/egp071)
- Willner, A., Thomson, S., Kröner, A., Wartho, J., Wijbrans, J.R., HERVÉ, F., et al. 2005, Time markers for the evolution and exhumation history of a Late Palaeozoic Paired Metamorphic Belt in North–Central Chile (34°–35°30'S): *Journal of Petrology*, v. 46, no. 9, p. 1835–1858. doi:[10.1093/petrology/egi036](https://doi.org/10.1093/petrology/egi036)
- Wu, C., 2015, Revised empirical garnet–biotite–muscovite–plagioclase geobarometer in metapelites: *Journal of Metamorphic Geology*, v. 33, no. 2, p. 167–176. doi: [10.1111/jmg.12115](https://doi.org/10.1111/jmg.12115)
- Zalba, P., Manassero, M., Laverret, E., Beaufort, D., Meunier, A., Morosi, M., and Segovia, L., et al. 2007, Middle Permian telodiagenetic processes in Neoproterozoic sequences, Tandilia System, Argentina: *Journal of Sedimentary Research*, v. 77, no. 6, p. 525–538. doi:[10.2110/jsr.2007.049](https://doi.org/10.2110/jsr.2007.049)
- Zi, J.-W., Muhling, J., and Rasmussen, B., 2024, Geochemistry of low-temperature (<350°C) metamorphic and hydrothermal monazite: *Earth-Science Reviews*, v. 249, p. 104668. doi:[10.1016/j.earscirev.2023.104668](https://doi.org/10.1016/j.earscirev.2023.104668)